SCIENCE CHINA Materials

REVIEWS

mater.scichina.com link.springer.com

Published online 17 October 2017 | https://doi.org/10.1007/s40843-017-9095-4

Sci China Mater 2018, 61(2): 185–209

SPECIAL ISSUE: Innovative Electrode Materials for Supercapacitors

Hierarchically nanostructured transition metal oxides for supercapacitors

Mingbo Zheng, Xiao Xiao, Lulu Li, Peng Gu, Xiao Dai, Hao Tang, Qin Hu, Huaiguo Xue and Huan Pang*

ABSTRACT **Highly efficient, clean, and sustainable electrochemical energy storage technologies have been investigated extensively to counter the shortage of fossil fuels and increasingly prominent environmental problems. Supercapacitors (SCs) have received wide attention as critical devices for electrochemical energy storage because of their rapid charging–discharging capability and long life cycle. Various transition metal oxides (TMOs), such as MnO_2, NiO, Co_3O_4, and CuO, have been extensively studied as electrode materials for SCs. Compared with carbon and conducting polymers, TMO materials can achieve higher specific capacitance. For further improvement of electrochemical performance, hierarchically nanostructured TMO materials have become a hot research area for electrode materials in SCs. The hierarchical nanostructure can not only offer abundant accessible electroactive sites for redox reactions but also shorten the ion diffusion pathway. In this review, we provide an overall summary and evaluation of the recent progress of hierarchically nanostructured TMOs for SCs, including synthesis methods, compositions, structures, and electrochemical performances. Both single-phase TMOs and the composites based on TMOs are summarized. Furthermore, we also prospect the developing foreground of this field. In this view, the important directions mainly include: the nanocomposites of TMOs materials with conductive materials; the cobalt-based materials and the nickel-based materials; the improvement of the volume energy density, the asymmetric SCs, and the flexible all-solid-state SCs.**

Keywords: hierarchical nanostructure, transition metal oxides, supercapacitors

INTRODUCTION

With the rapid development of global economy, energy shortage and environmental pollution have become two extremely important issues worldwide. A breakthrough in exploiting highly efficient and clean energy storage technologies is necessary to satisfy future energy requirements [1–6]. The electrochemical energy storage is the most promising approach because of its high efficiency, good reliability, ease of operation, and good eco-friendly character [7–18]. Electrochemical energy storage technologies mainly include batteries and supercapacitors (SCs) [19,20]. As a new energy storage approach, SCs combine the advantages of high energy density of rechargeable batteries and high power density of dielectric capacitors [19–29]. SCs have been regarded as highly important candidates for energy storage devices because of their fast charging–discharging capability, long cycle stability (>10^5 cycles), high power density (>10 kW kg^{-1}), low cost, environment-friendly nature, low maintenance, and safe operation [30–46]. In certain fields, SCs can partly or fully replace traditional batteries.

SCs can be divided into two categories according to energy storage mechanism: electrical double-layer capacitors (EDLCs) (Fig. 1a) and pseudocapacitors (Fig. 1b) [19–21]. The capacitance of EDLCs is associated with the charge separation and accumulation at the interface between electrode and electrolyte [19–21]. During charging, the electric charges on the surface of electrode attract the ions with opposite charges in the electrolyte. Thus, the electric double layer is formed on the surface of electrode and the energy stroge is realized. The capacitance stored in the electric double layer is proportional to the specific surface area of the electrode. During discharging, ions return to the electrolyte and electrons flow into the external circuit. Nanostructured carbon materials, such as mesoporous carbon, activated carbon, carbon nanotubes,

School of Chemistry and Chemical Engineering, Institute for Innovative Materials and Energy, Yangzhou University, Yangzhou 225009, China

* Corresponding author (emails: huanpangchem@hotmail.com or panghuan@yzu.edu.cn)

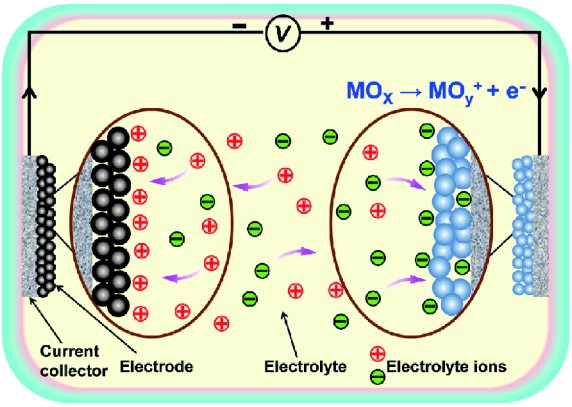

Figure 1 Schematic of the two different mechanisms of SCs: (a) EDLCs and (b) pseudocapacitors.

carbon nanofibers, and graphene, have been widely studied as the electrode materials of EDLCs. The capacitance of pseudocapacitors is derived from the fast and reversible Faradaic process (redox reactions) occurring on the surface or near surface of the electrode materials [19–21]. Although the generation process of pseudocapacitance involves redox reactions, it is different from the reaction process of battery. The battery is controlled by the ion diffusion within the crystalline framework of active material; while the pseudocapacitor is not limited by the diffusion process [19]. Therefore, the pseudocapacitor possesses highly dynamic reversibility and is more closer to the characteristics of the capacitor. The electrode materials of pseudocapacitors mainly include transition metal oxides (TMOs) and conductive polymers.

Conventional carbon material-based EDLCs usually exhibit low specific capacitance [19,20]. TMOs, which possess multiple oxidation states, could achieve markedly larger specific capacitance than carbon materials [19,20]. Early investigations on electrode materials have concentrated on noble TMOs, such as RuO_2 and IrO_2. RuO_2 with three oxidation states within 1.4 V, indicating a large specific capacitance of 2000 F g^{-1} [47,48]. However, the exceedingly high cost and environmentally poisonous nature limit their practical applications. Hence, cheap and high-performance TMOs, such as MnO_2, NiO, Co_3O_4, and CuO, have been extensively studied as the electrode materials for SCs [49–54]. Moreover, multiple-metal TMOs, such as $NiCo_2O_4$, $NiCoO_2$, and ZnV_2O_4, have also attracted considerable interest because these materials can provide better electrochemical performance compared with single-metal TMOs [55–57]. TMOs with a variety of structures and morphologies, such as thin films, nanowires/nanorods, nanotubes, nanosheets, nanoflowers, and hollow nanospheres, have been fabricated *via* different synthesis routes [49–60]. Moreover, their electrochemical properties have been extensively investigated.

Hierarchically nanostructured materials are self-assembly systems that are assembled from low dimensional nanobuilding blocks, such as nanoparticles (NPs), nanowires, nanorods, nanotubes, and nanosheets [61,62]. Recently, hierarchically nanostructured TMO materials have gradually become a research hotspot in SC field because of their unique structures [63–67]. These structures could offer large specific surface area, abundant accessible electroactive sites, and short ion diffusion pathway during the rapid charge–discharge process [63–67]. Hierarchically nanostructured TMOs exhibit higher power properties, larger specific capacitances, and more outstanding cycle stabilities compared with common TMOs. In this review, we mainly expound the topic of hierarchically nanostructured TMO electrode materials for SCs. The synthesis and electrochemical performance of hierarchically nanostructured single- or multiphase TMOs are systematically reviewed. We emphasize on several advanced TMO-based composite materials with excellent electrochemical properties, which mainly originate from advantageous compositional and structural characteristics. In addition, we propose several personal prospects to motivate further development of hierarchically nanostructured TMOs for SCs.

The following sections describe the hierarchically nanostructured TMOs as electrode materials for SCs. The summary mainly is divided into two parts: one is single-phase TMOs, and the other is the composites based on TMOs. Unless otherwise noted, the electrochemical tests are mainly investigated in three-electrode systems. The electrolytes for all works are shown in parentheses.

HIERARCHICALLY NANOSTRUCTURED SINGLE-PHASE TMOs FOR SCs

Manganese oxides

Electrochemical SCs based on manganese dioxide (MnO_2) have attracted considerable interest because of its rich polymorphisms (α-, β-, γ-, δ-, λ-, and ε-type), high theoretical specific capacitance, high natural abundance, and good environmental compatibility [68–75].

Flower-like hierarchical α-MnO_2 sub-microspheres were successfully fabricated by Yuan and coworkers *via* a novel interfacial strategy [76]. The Brunauer–Emmett–Teller (BET) specific surface area of the α-MnO_2 sample is 216 m^2 g^{-1}. To evaluate electrochemical performance, the hierarchical α-MnO_2 material was investigated *via* cyclic

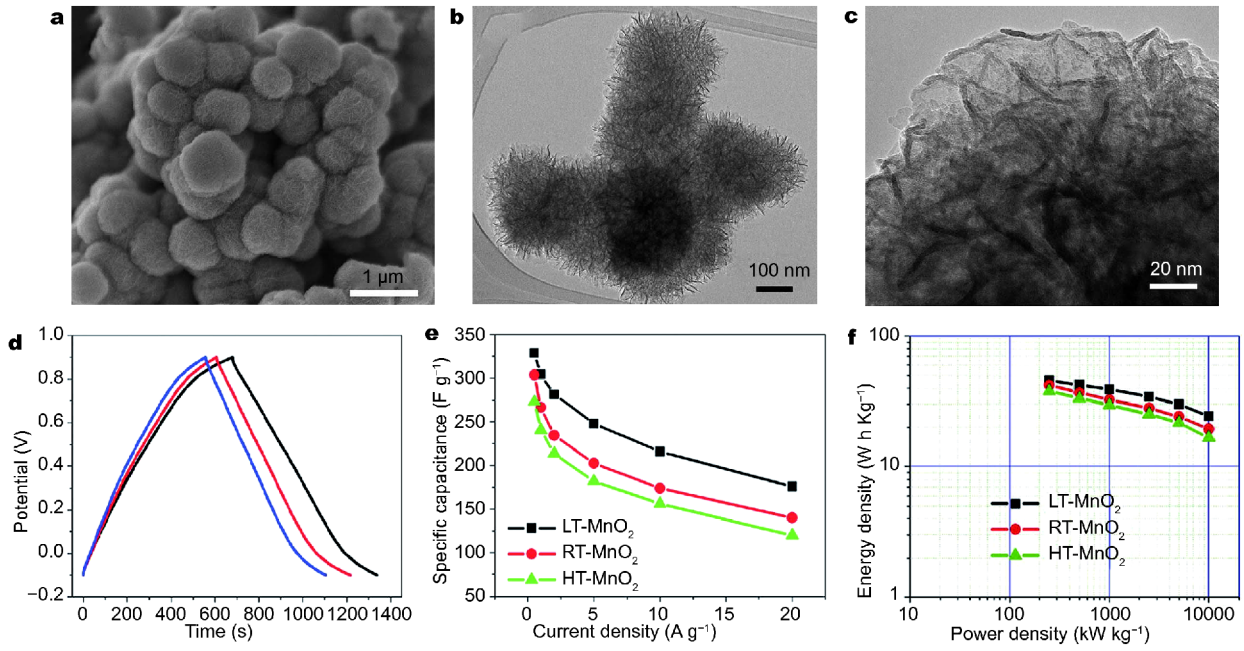

Figure 2 (a) SEM and (b), (c) TEM images of the LT-MnO_2. Electrochemical properties of the three samples; (d) galvanostatic charge–discharge curves at 0.5 A g^{-1}; (e) specific capacitances at various current densities; (f) Ragone plots. Reproduced with permission from Ref. [79]. Copyright 2012, the Royal Society of Chemistry.

voltammetry (CV), cyclic chronopotentiometry (CC), and electrochemical impedance spectroscopy in 1 mol L^{-1} K_2SO_4. The electrochemical measurement results in high specific capacitances of 298 and 236 F g^{-1} at 0.117 and 2.353 A g^{-1}, respectively. Furthermore, the α-MnO_2 sample shows 90% retention after 2,000 cycles at 2 A g^{-1}. The good performance is ascribed to the special hierarchical structure and rich MnO_2-electrolyte interfaces.

Lee *et al.* [77] prepared hierarchical nanostructures of hydrated α-MnO_2 by one-step synthesis at room temperature. The α-MnO_2 sample consists of small ultrathin nanorod-like structures with diameters of 2–4 nm. The MnO_2 electrode delivers a high specific capacitance of 356 F g^{-1} at 2 A g^{-1} (1 mol L^{-1} Na_2SO_4). After 2,000 cycles of cycling test, no capacitance degradation is observed.

β-MnO_2 as electrode material in SCs is also investigated. Zhao *et al.* [78] successfully fabricated hierarchical porous β-MnO_2 nanoflowers assembled by ultrathin nanoplates at room temperature. The BET specific surface area of the β-MnO_2 sample is as high as 267 m^2 g^{-1}. The electrochemical measurements demonstrate that the sample possesses a large energy density of 22.6 W h kg^{-1} at a high power density of 9.1 kW g^{-1}, with a high specific capacitance of 201.5 F g^{-1} (1 mol L^{-1} Na_2SO_4). Furthermore, at 2 mV s^{-1}, the specific capacitance reaches up to 296.3 F g^{-1}, which is evidently superior to those of β-MnO_2 powders (~7 F g^{-1}) and β-MnO_2 nanorods (14.9 F g^{-1}).

Using a simple and scalable method, Li *et al.* [79] prepared hierarchical MnO_2 nanostructures assembled by ultrathin nanoflakes. The resulting products labeled as LT-MnO_2, RT-MnO_2, and HT-MnO_2 (LT, RT, and HT represent low temperature, room temperature, and high temperature, respectively) were synthesized by conducting the reaction in an ice bath, at room temperature, and at 100 °C. Scanning electron microscopy (SEM) and transmission electron microscopy (TEM) images of LT-MnO_2 are shown in Fig. 2a–c. The MnO_2 nanospheres are assembled by small nanoflakes with low crystallinity. The LT-MnO_2 displays the largest specific surface area (269.0 m^2 g^{-1}) compared with the RT-MnO_2 (173.6 m^2 g^{-1}) and HT-MnO_2 (164.6 m^2 g^{-1}). In addition, the LT-MnO_2 possesses the highest specific capacitance (176 F g^{-1}) at 20 A g^{-1} (1 mol L^{-1} Na_2SO_4) compared with the RT-MnO_2 (140 F g^{-1}) and HT-MnO_2 (120 F g^{-1}) (shown in Fig. 2d, e). As shown in Fig. 2f, at a power density of 250 W kg^{-1}, the LT-MnO_2 also shows the highest energy density of 45.6 W h kg^{-1} among the three samples (RT-MnO_2 with 42.2 W h kg^{-1} and HT-MnO_2 with 37.9 W h kg^{-1}) [76–79].

Raj *et al.* [80] synthesized hierarchical mesoporous δ-MnO_2 *via* an easy single-step and template-free method.

This hierarchical mesoporous δ-MnO_2 has a large BET specific surface area of 238 $m^2 g^{-1}$. The specific capacitance of δ-MnO_2 is 364 F g^{-1} at 1 A g^{-1} (1 mol L^{-1} Na_2SO_4). Furthermore, the asymmetric SCs device with a large voltage window of 0–2 V was fabricated by using δ-MnO_2 as the cathode and activated carbon as the anode. The device shows a specific capacitance of 86.5 F g^{-1} at 1 A g^{-1} and a capacitance retention of 100% after 3,000 cycles at 20 A g^{-1}. The device exhibits a high energy density of 48.06 W h kg^{-1} at a power density of 1.0 kW kg^{-1}.

Cobalt oxides

Among TMOs, Co_3O_4 is also considered as a highly promising material due to its cost effectiveness, environmental benignancy, and ultrahigh theoretical specific capacitance (3560 F g^{-1}) [81–84]. Cobalt oxides with a variety of structures and morphologies, such as NPs [85], nanowires [86], nanorods [87], nanosheets [88], and porous nanostructures [89,90], have been fabricated *via* electrochemical and/or chemical routes, and the corresponding electrochemical performance is under intensive investigation.

A hydrothermal strategy based on a self-assembled monolayer polystyrene sphere template was used by Cao *et al.* [91] for the fabrication of hierarchical porous Co_3O_4 film. The Co_3O_4 film is approximately 20 nm thick. The specific capacitances of the Co_3O_4 films are 352 and 291 F g^{-1} at 2 and 40 A g^{-1} (2 mol L^{-1} KOH), respectively. These specific capacitances are higher than that of the sample obtained without using a template (325 and 217 F g^{-1} at 2 and 40 A g^{-1}).

Xiao *et al.* [92] prepared three-dimensional (3D) enoki mushroom-like Co_3O_4 hierarchitectures *via* an easy reflux method. The primary structure of Co_3O_4 hierarchitectures is the nanowire with a diameter of approximately 3.2 μm. Each Co_3O_4 nanowire is made up of numerous Co_3O_4 NPs. The Co_3O_4 material displays a large specific capacitance of 787 F g^{-1} at 1 A g^{-1} (6 mol L^{-1} KOH), and a capacity retention of 94.5% after 1,000 cycles at 10 A g^{-1}. The asymmetric SCs device (carbon mateials as anode) exhibits an energy density of 23.9 W h kg^{-1} at 0.5 A g^{-1}, together with a power density of 0.375 kW kg^{-1}. The unique 3D enoki mushroom-like hierarchitectures could evidently improve the rate of ion diffusion and the stability of electrodes, which results in considerable electrochemical performances of the Co_3O_4 material.

Qu *et al.* [93] reported that hollow fluffy cages (HFC) of Co_3O_4 were prepared by the formation of $Co(OH)_2$ hollow cages and subsequent calcination at different temperature. The HFC of Co_3O_4 was annealed at 250, 300, and 400°C, respectively. The synthetic scheme for HFC Co_3O_4 is shown in Fig. 3a. The TEM image of Cu_2O template (Fig. 3b) displays a polyhedron structure with a size of ~250 nm. As shown in Fig. 3c, the size of the internal voids of the as-prepared hollow cages is ~250 nm, which is inherited from the dimensions of the Cu_2O templates. As evidenced in the TEM image (Fig. 3d), the morphology of the HFC-like nanostructure is excellently preserved after annealing at 250°C. The specific surface area of HFC-250 is approximately 245.5 $m^2 g^{-1}$, which is substantially higher than those of HFC-300 (120 $m^2 g^{-1}$) and HFC-400 (67.3 $m^2 g^{-1}$). The nearly symmetric charge-discharge curves imply that the HFC-250 delivers high coulombic efficiency and low polarization (Fig. 3e). At 1 A g^{-1} (shown in Fig. 3f), the HFC-250 electrode possesses the largest specific capacitance (948.9 F g^{-1}), which is markedly larger than those of HFC $Co(OH)_2$ (400.7 F g^{-1}), HFC-300 (489.9 F g^{-1}), HFC-400 (297 F g^{-1}), and Co_3O_4-common (151.3 F g^{-1}) electrodes (2 mol L^{-1} KOH). Furthermore, the HFC-250 exhibits superior rate performance (Fig. 3g) and good cycle stability.

Nickel oxides

Nickel oxides have been widely studied in SCs field because of their high theoretical capacity (2573 F g^{-1}), cost effectiveness, and environmental friendliness [94–99]. By an easy hydrothermal method, Hu *et al.* [100] designed and synthesized hierarchical NiO nanosheets/nanowires with Ni foam substrate. The specific capacitances of the electrodes are 1493 and 867 F g^{-1} at 3 and 50 A g^{-1} (6 mol L^{-1} KOH), respectively, which are superior to those of the mesoporous NiO nanosheets (1250 and 633 F g^{-1} at 3 and 50 A g^{-1}, respectively). Furthermore, the unique hierarchical NiO nanosheet/nanowire electrodes exhibit good rate performance and good cycling stability.

Using a successive electrode-position method with ZnO nanorods as template on Ni foam, Cao *et al.* [101] synthesized 3D hierarchical NiO nanotube arrays. Fig. 4a shows the schematic for synthesizing this material. As seen in the SEM and TEM (Fig. 4b, c) images, the sample is consisted of interconnected branch nanoflakes (~10 nm), and the diameter of nanotube is ~170 nm. Owing to the special hierarchical porous structure, the NiO nanotube arrays show high specific capacitances of 675 and 569 F g^{-1} at 2 and 40 A g^{-1} (1 mol L^{-1} Na_2SO_4) (Fig. 4g), respectively. The pseudocapacitive performance of NiO nanotube arrays on Ni foil and Ni foam were also

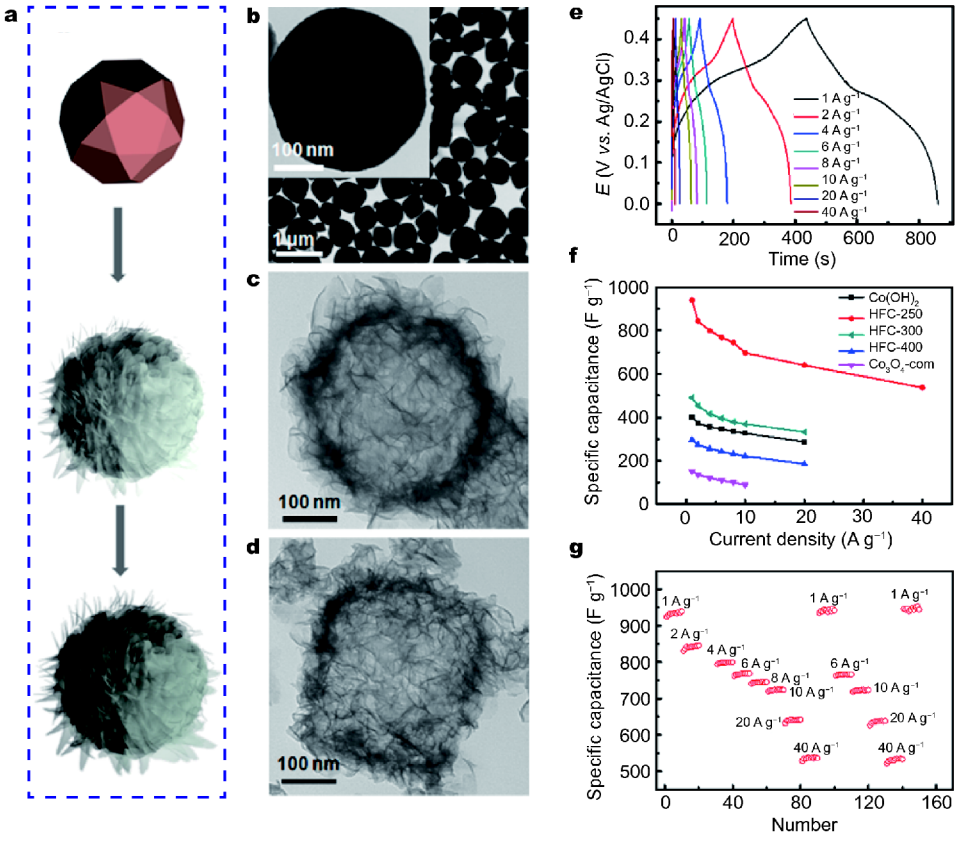

Figure 3 (a) Schematic of the preparation of $Co(OH)_2$ and Co_3O_4. TEM images for (b) Cu_2O template, (c) $Co(OH)_2$, and (d) Co_3O_4. (e) Charge–discharge curves of the HFC-250 electrode. (f) Plots of the specific capacitance of $Co(OH)_2$, HFC-250, HFC-300, HFC-400, and Co_3O_4-com. (g) Rate capability of the HFC-250 electrode when the current density was progressively varied. Reproduced with permission from Ref. [93]. Copyright 2015, the American Chemical Society.

compared. The specific capacitance of the NiO on the Ni foil is 495 F g^{-1} at 2 A g^{-1}, which is lower than that of the NiO on Ni foam (675 F g^{-1} at 2 A g^{-1}). The porous NiO arrays on Ni foam electrode demonstrate a low loss of 6.8% after 10,000 cycles at 2 A g^{-1}. This excellent electrochemical performance can be ascribed to the hierarchical porous architecture with large reaction surface area and fast ion transfer. This synthesis method can potentially be applied to the fabrication of other TMO nanotube arrays.

Multi-shell self-assembled hollow structure materials are also investigated in SCs. Zhu *et al.* [102] designed and prepared single-, double-, and triple-shelled NiO (S–NiO, D–NiO, and T–NiO, respectively) hollow nanospheres by a controllable layer-by-layer self-assembly method with the calcination of $Ni(OH)_2$/C precursors. The BET specific surface area of the D–NiO is approximately 92.99 m^2 g^{-1}, which is higher than those of T–NiO (23.45 m^2 g^{-1}) and S–NiO (61.63 m^2 g^{-1}). The average pore sizes for S–NiO, D–NiO, and T–NiO are 18.24, 7.04, and 12.30 nm, respectively. The electrochemical measurements indicate that the D–NiO possesses the highest specific capacitance of 612.5 F g^{-1} compared with S–NiO (432.2 F g^{-1}) and T–NiO (292.4 F g^{-1}) at 0.5 A g^{-1} (2 mol L^{-1} KOH). The D–NiO also exhibits good cyclic performance, with capacitance retention exceeding 90% after 1,000 cycles.

Using a facile, low-cost, and environment-friendly template method, Liu *et al.* [103] successfully prepared hierarchical mesoporous NiO nanoarrays (NiO–HMNAs). The synthesis process of NiO–HMNAs is shown in Fig. 4d. The edge length of NiO–HMNAs is 1.6 μm (shown in Fig. 4e, f). The average thickness of NiO–HMNAs is ~10 nm (Fig. 4f, inset). As a battery-type electrode for hybrid SCs, the specific capacitance of NiO–HMNAs is 3114 F g^{-1} at 5 mA cm^{-2} (2 mol L^{-1} KOH). Furthermore, the optimized hybrid SC device demonstrates a high energy density of 67.0 Wh kg^{-1} at a power

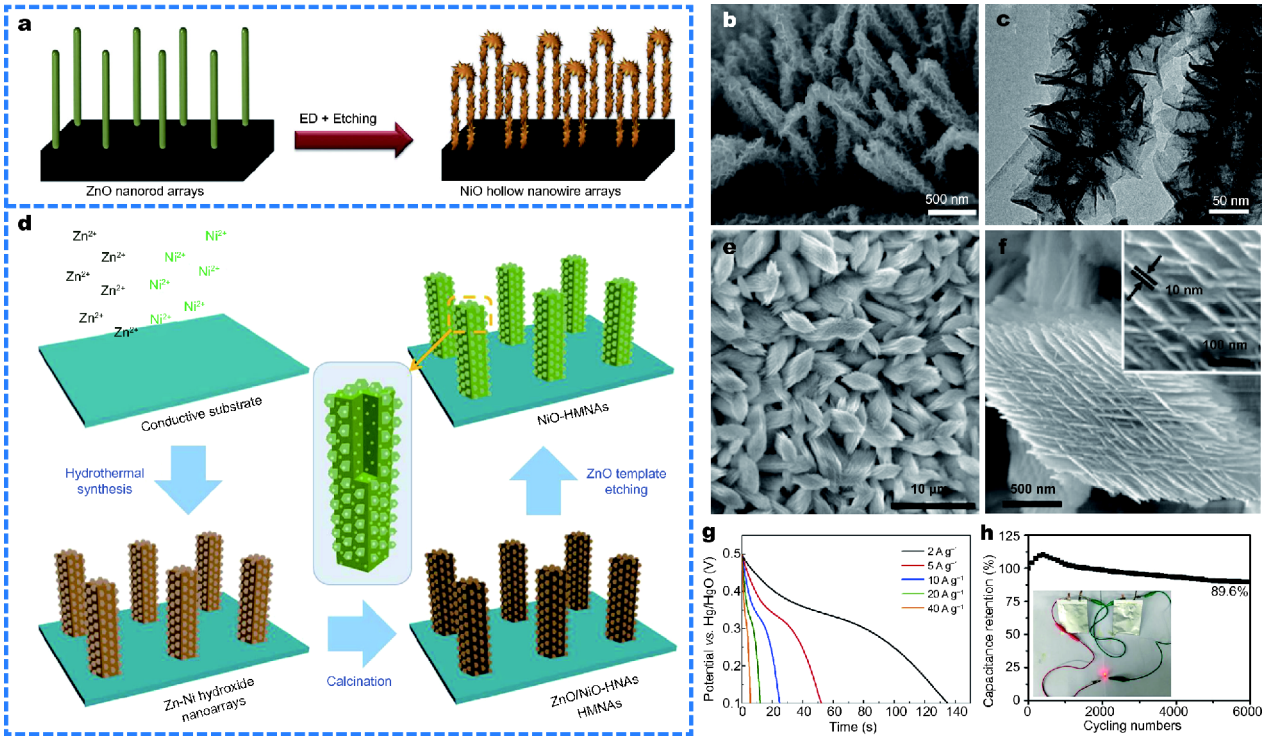

Figure 4 (a) Schematic of the preparation of hierarchical NiO nanotube arrays on Ni foam. (b) SEM image of NiO nanotube arrays on Ni foam. (c) TEM image of NiO nanotube. (d) Schematic of the preparation of NiO–HMNAs on Cu foam. (e) and (f) SEM images of NiO–HMNAs. (g) Discharge curves of NiO nanotube arrays on Ni foam. (h) Cycling performance of the hybrid SC device based on NiO–HMNAs. Reproduced with permission from Ref. [101]. Copyright 2014, Elsevier. (d–f, h) Reproduced with permission from Ref. [103]. Copyright 2016, Elsevier.

density of 320 W kg^{-1} and a good capacitance retention of 89.6% after 6,000 cycles (Fig. 4h). The ultrahigh specific capacitance of NiO–HMNAs is ascribed to the unique hierarchical mesoporous architecture.

Copper oxides

Copper oxide can be considered as another promising candidate for SCs because of its non-toxicity, abundance, and facile preparation [104,105]. Through a facile electrochemical process, 3D nanostructured CuO electrodes were prepared for SCs by Chen *et al.* (Fig. 5a, b) [106]. Due to its unique nanostructure, the as-prepared CuO nanoribbon-on-Ni-nanoporous/Ni foam (CNRNP) electrodes show excellent energy storage performance relative to a traditional electrode. Ni foam and flat Ni are also respectively used as substrate to fabricate general copper oxide samples. On the Ni foam, CuO nanoflakes (CNFNF) form a thick and uniform film, completely covering the Ni foam framework (Fig. 5c). On the flat Ni plate, the flake-like CuO (FLC) is formed (Fig. 5d). The specific capacitance of the CNRNP electrode is 800 F g^{-1} at 200 mV s^{-1} (3 mol L^{-1} KOH), which retains 91% compared with that at 10 mV s^{-1} (Fig. 5e, f). By contrast, the CNFNF and FLC electrodes deliver 81% and 69% of that at 10 mV s^{-1}, respectively. The symmetric triangular shape of charge–discharge curves indicates that the CNRNP possesses satisfactory pseudocapacitive behavior (Fig. 5g).

An easy and low-cost one-step surface oxidation process was applied by Zhao *et al.* [107] for the preparation of 3D flower-like CuO hierarchical structures grown on Cu foam. Given the innovative synthesis method and 3D connect/quasi-connect structures, this sample gains considerable attention as binder-free electrode material for SCs. The 3D flower-like CuO/Cu foam electrode could offer abundant active sites for redox reactions, effectively promote electrolyte penetration, enhance electronic conductivity, and shorten ion diffusion pathway. The specific capacitances of CuO are calculated to be 1641.4 and 1266.7 mF cm^{-2} at 2 and 20 mA cm^{-2} (5 mol L^{-1} NaOH), respectively.

By an alkaline solution oxidation, Luo *et al.* [108] successfully synthesized CuO nanostructures with different surfactants (sodium dodecyl sulfate (SDS) and poly-

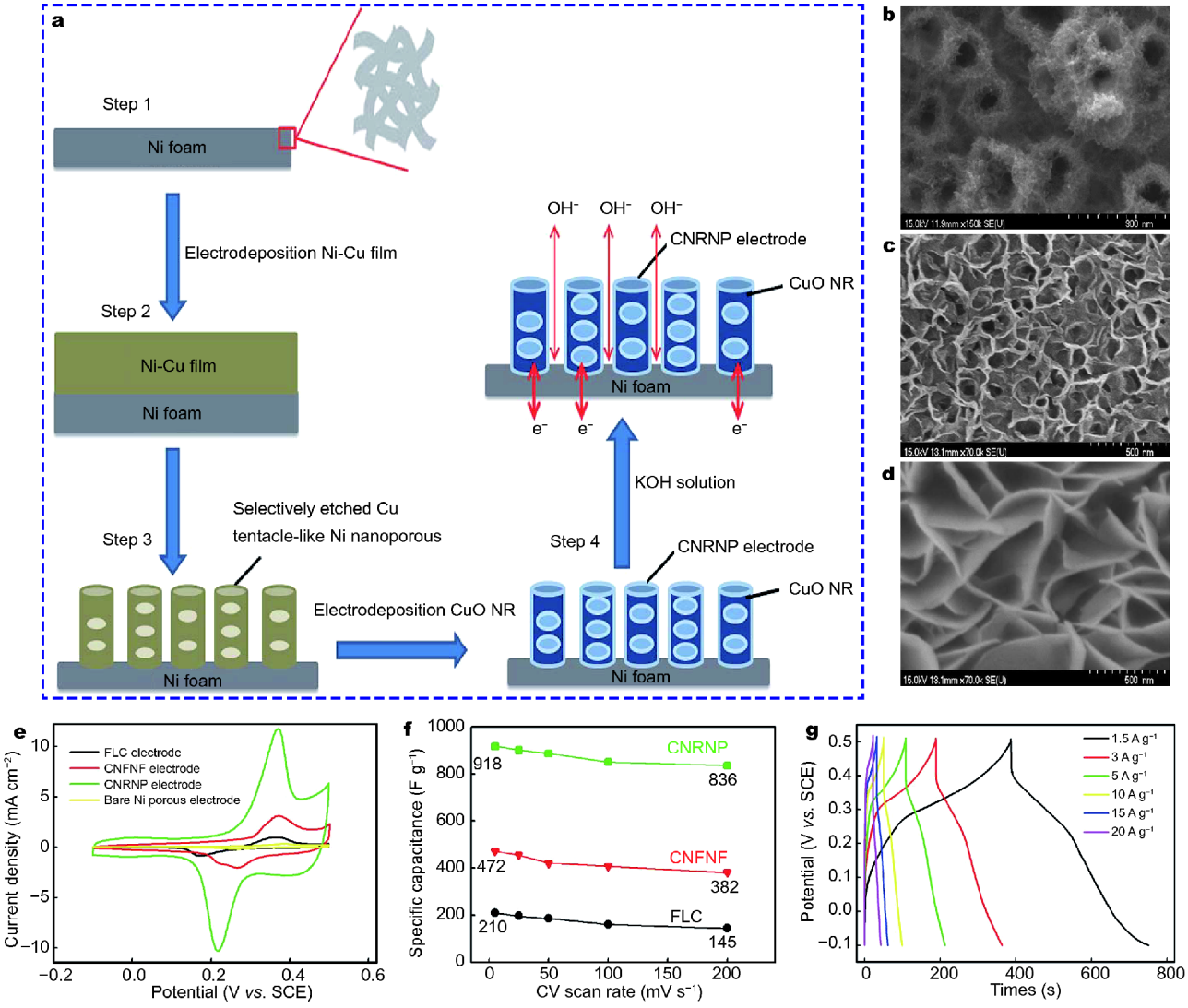

Figure 5 (a) Schematic of the preparation of CNRNP electrode; SEM images of (b) CNRNP, (c) CNFNF, and (d) FLC; (e) CV curves of all samples at 10 mV s^{-1}; (f) specific capacitance of all samples at different scan rates; (g) charge-discharge curves of CNRNP. Reproduced with permission from Ref. [106]. Copyright 2014, the Royal Society of Chemistry.

vinyl alcohol (PVA)). The CuO electrode obtained with SDS shows superior electrochemical performance because of its ultrathin nanoleaves, which constitute a flower-shaped nanostructure, and possesses specific capacitances of 520 and 405 F g^{-1} at 1 and 60 A g^{-1} (1 mol L^{-1} KOH), respectively, and a capacitance retention of 95.2% after 5,000 cycles at 1 A g^{-1}.

Bismuth oxides

Owing to abundant crystal morphologies and unique physical properties, Bi_2O_3 has attracted extensive attention in SC field [109]. Bi_2O_3 presents five main polymorphic forms (α-, β-, γ-, δ-, and ω-Bi_2O_3). Among these forms, the high-temperature δ and low-temperature α phases are stable [110–112]. Gujar *et al.* first reported that Bi_2O_3 thin film, as positive electrode material for SCs, possessed a low specific capacitance of only 98 F g^{-1} but exhibited high electrochemical reversibility [112].

Tong *et al.* [113] reported that hierarchical rippled Bi_2O_3 nanobelts were synthesized *via* an electrode-position method. The Bi_2O_3 nanobelts possess a width of 250–300 nm, a length of 1–5 μm, and a thickness of 10–30 nm. The intervals between the ripples are approximately 15–30 nm. The BET specific surface area of hierarchical Bi_2O_3 nanobelts sample (196 m^2 g^{-1}) is 8 times of that of Bi_2O_3 nanobelts sample with smooth surfaces (24 m^2 g^{-1}).

The specific capacitance of the hierarchical rippled Bi_2O_3 nanobelts is 250 F g^{-1} at 100 mV s^{-1} (1 mol L^{-1} Na_2SO_4), which is remarkablely larger than the Bi_2O_3 nanobelts with smooth surfaces (61 F g^{-1}).

An easy one-step precipitation approach with the addition of diverse surfactants was used by Yuan's group for the synthesis of rod-like Bi_2O_3 [114]. The surfactants with various chain structures can effectively regulate and control the morphologies of Bi_2O_3 products. The Bi_2O_3 sample synthesized using P123 surfactant as electrode material was investigated. The sample exhibits a large specific capacitance of 1350 F g^{-1} at 0.1 A g^{-1} (6 mol L^{-1} KOH), excellent rate performance (71.4% retention from 0.1 to 2 A g^{-1}), and an outstanding cycle performance (only 2.4% capacitance fade after 1,000 cycles).

Nickel cobalt oxides

Bimetallic oxides usually offer higher electrochemical activity than single metal oxides [115–117]. Nickel cobaltite exhibits excellent electrochemical performance because of richer redox reaction between nickel and cobalt ions [118]. A variety of nickel cobaltite materials with different morphologies, such as NPs [119], nanowires [120,121], urchin-like shape [122], and hollow spheres [123], have been studied as electrode materials for SCs.

To shorten the synthesis time, Xiao *et al.* [124] reported a template-free microwave-assisted heating reflux method to prepare 3D hierarchical flower-shaped $NiCo_2O_4$ microspheres. The $NiCo_2O_4$ microspheres are constituted of numerous flower-shaped nanostructures. The flower-shaped $NiCo_2O_4$ microspheres demonstrate a high specific capacitance of 1006 F g^{-1} at 1 A g^{-1} (6 mol L^{-1} KOH) and good cycle performance (retention of 93.2% after 1,000 cycles at 8 A g^{-1}).

The design and preparation of novel nanomaterials have gradually become the core research in optimizing pseudocapacitive performance. Li *et al.* [125] reported that the $NiCo_2O_4$ multiple hierarchical structures (MHSs) composed of two-dimensional (2D) nanosheets and one-dimensional (1D) nanowires were directly anchored on Ni foam (Fig. 6a). First, the $NiCo_2O_4$ nanowires (NCO1) that uniformly covered the substrate were formed by a hydrothermal process followed by annealing treatment. After that, by a second hydrothermal process, the NCO1 was transformed into $NiCo_2O_4$ MHSs, which was named as NCO2. The nanowire was found to be superior over the high-dimensional nanosheet in the growth order; thereby effectively promoting the integration of these different nanostructures into the $NiCo_2O_4$ MHSs. As shown in Fig. 6b, c, the $NiCo_2O_4$ MHSs with diameters of about 4–6 μm were obtained. All microspheres possess a 3D structure, in which the 2D nanosheets form the skeleton of microspheres, while the 1D nanowires surround the nanosheet. Given the favorable mesoporous architecture and large specific surface area, the sample NCO2 ($NiCo_2O_4$ MHSs) shows the highest specific capacitance of 2623.3 F g^{-1} at 1 A g^{-1} (3 mol L^{-1} KOH) (Fig. 6d). A capacity retention of 68% can be achieved from 1 A g^{-1} to 40 A g^{-1}. The sample also displays good stability with 94% retention after 3,000 cycles at 10 A g^{-1}.

By a mild solution approach with polymeric nanotubes (PNT) as the template, Yu *et al.* [126] successfully fabricated hierarchical $NiCoO_2$ nanotubes composed of nanosheets. Fig. 6e displays the SEM image of $NiCoO_2$ nanotubes obtained after calcination of the Ni-precursor@PNT composite at 400°C. As shown in Fig. 6f, the mesoporous $NiCoO_2$ nanosheet–nanotube structures possess hierarchical external construction and hollow internal structure with a diameter of approximately 100 nm. When tested at 2, 4, 8, 10, 20, and 40 A g^{-1} (2 mol L^{-1} KOH), the $NiCoO_2$ nanotube electrodes show high specific capacitances of 1468, 1352, 1233, 1178, 1020, and 672 F g^{-1}, respectively. At 10 A g^{-1}, the specific capacitance is 1178 F g^{-1} in the first cycle. The specific capacitance gradually decreases to 1168 F g^{-1} after 3,000 cycles, resulting in only 0.8% loss of overall capacitance. Furthermore, the $NiCoO_2$ nanotubes show virtually 100% of the coulombic efficiency during the whole cycle (Fig. 6g). This excellent performance of the $NiCoO_2$ nanotubes is ascribed to the porous and hierarchical structures, which provide more effective contact areas between the active materials and electrolyte ions. Moreover, the wide-open ends of the $NiCoO_2$ nanotubes provide extra paths for the electrolyte.

Zinc vanadium oxides

Cao *et al.* [127] designed a simple and template-free approach to fabricate hierarchical nanospheres (NHNs) of ZnV_2O_4. As shown in Fig. 7a, b, these nanospheres are composed of extremely thin nanosheets. Fig. 7c demonstrates the crystal geometry of spinel oxide ZnV_2O_4. Fig. 7d shows that the specific capacitances of ZnV_2O_4 NHNs are 385, 360, 324, and 272 F g^{-1} at current densities of 0.5, 1, 2, and 4 A g^{-1}, respectively. Furthermore, the ZnV_2O_4 NHNs electrode exhibits good cycle stability with 89% of capacity retention after 1,000 cycles at 1 A g^{-1}.

HIERARCHICALLY NANOSTRUCTURED COMPOSITES BASED ON TMOs FOR SCs

Multiphase composites based on TMOs could effectively

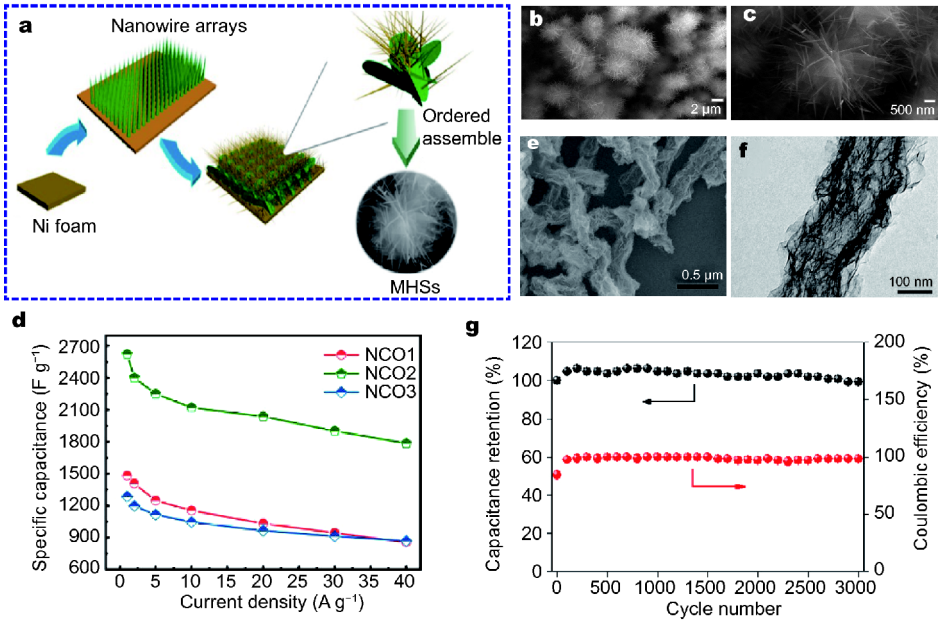

Figure 6 (a) Schematic of the preparation of $NiCo_2O_4$ MHSs; (b and c) FESEM images of the $NiCo_2O_4$ MHSs (NCO2) on Ni foam; (d) specific capacitance obtained from the discharge curves; (e) SEM image and (f) TEM image of the hierarchical $NiCoO_2$ nanosheets; (g) cycling performance of $NiCoO_2$ at 10 A g^{-1}. (a, d) Reproduced with permission from Ref. [125]. Copyright 2014, the American chemical Society. (e–g) Reproduced with permission from Ref. [126]. Copyright 2014, Elsevier.

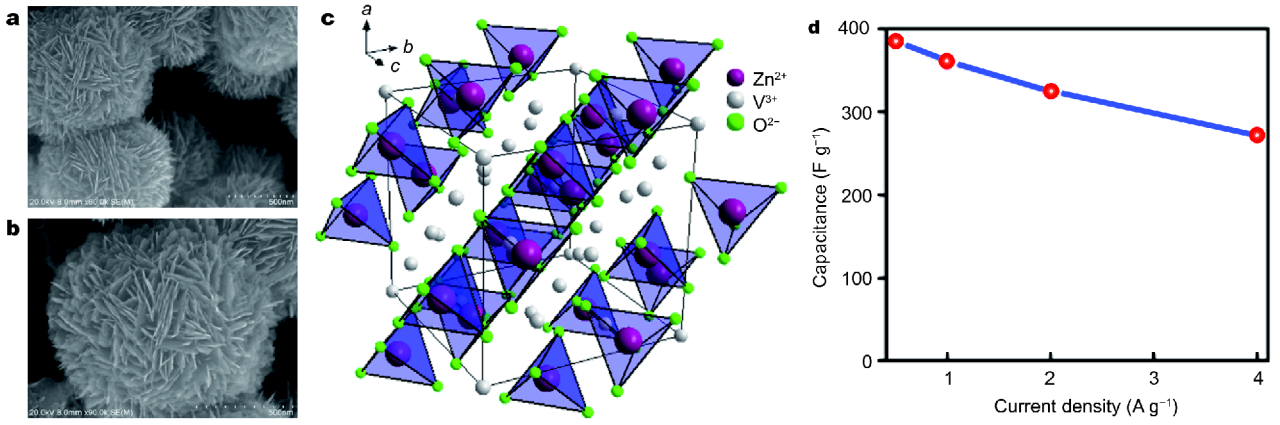

Figure 7 (a and b) SEM images of ZnV_2O_4 NHNs; (c) crystal structure of spinel ZnV_2O_4 with corresponding atoms; (d) capacitance as a function of current density. Reproduced with permission from Ref. [127]. Copyright 2014, the American Chemical Society.

improve the specific capacitance and cycling performance of the devices compared with single-phase TMOs because of the complex chemical compositions and the synergetic effect of both individual components [128–135]. In the following section, four types of composites were introduced, namely: 1) composites of manganese oxides and other TMOs; 2) composites of gold NP-doped TMOs; 3) composites of carbon materials and TMOs; and 4) other forms of TMOs composites.

Composites of manganese oxides and other TMOs

Lee *et al.* [136] designed and synthesized binder-free 3D CoO@MnO_2 core–shell nanohybrids by using a facile method (shown in Fig. 8a). The 3D CoO@MnO_2 core–shell structure has a diameter of 268 nm (Fig. 8b). The 3D CoO@MnO_2 core–shell nanohybrid electrode delivers

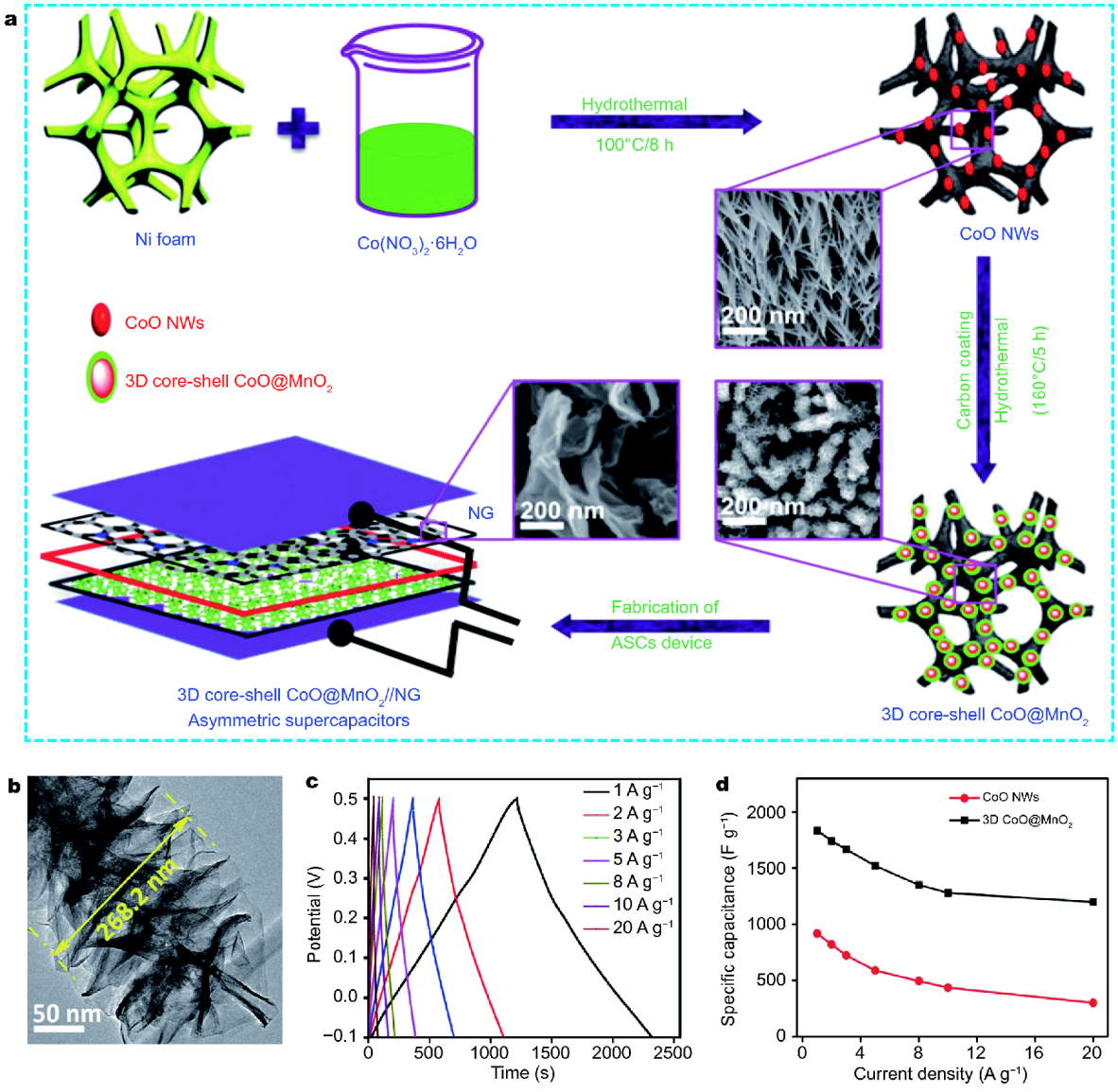

Figure 8 (a) Schematic of the preparation of 3D CoO@MnO_2 nanohybrid; (b) TEM image of the 3D CoO@MnO_2; (c) charge–discharge curves of the CoO@MnO_2; (d) cycle stabilities of the 3D CoO@MnO_2 core–shell nanohybrid and CoO NWs at 5 A g^{-1}. Reproduced with permission from Ref. [136]. Copyright 2017, the Royal Society of Chemistry.

good electrochemical performance with high specific capacitances (1835 and 1198 F g^{-1} at 1 and 20 A g^{-1}) (6 mol L^{-1} KOH) (Fig. 8c, d), and outstanding cycle performance (97.7% capacitance retention after 10,000 cycles at 1 A g^{-1}). When this 3D CoO@MnO_2 core–shell nanohybrid was used as cathode and assembled into an asymmetric SCs combined with a N-doped graphene anode, the formed asymmetric SCs device shows a high specific capacitance of 191 F g^{-1} at 1 A g^{-1} and good cycle performance with 86.8% retention after 10,000 cycles. The device presents an energy density of about 85.9 W h kg^{-1} at a power density of 852.4 W kg^{-1}.

Meng *et al.* [137] fabricated hierarchically densely packed porous MnO_2 microspheres doped with Fe_3O_4 NPs through a one-step low-cost ultrasound-assisted method. The SEM and TEM images (Fig. 9a, b) show that the sample owns a unique hierarchical nanostructure. The microsphere is composed of numerous randomly interconnected nanoflakes. The Fe_3O_4–MnO_2 electrode shows a capacitance of 367.4 F g^{-1} at 100 mV s^{-1} (1 mol L^{-1}

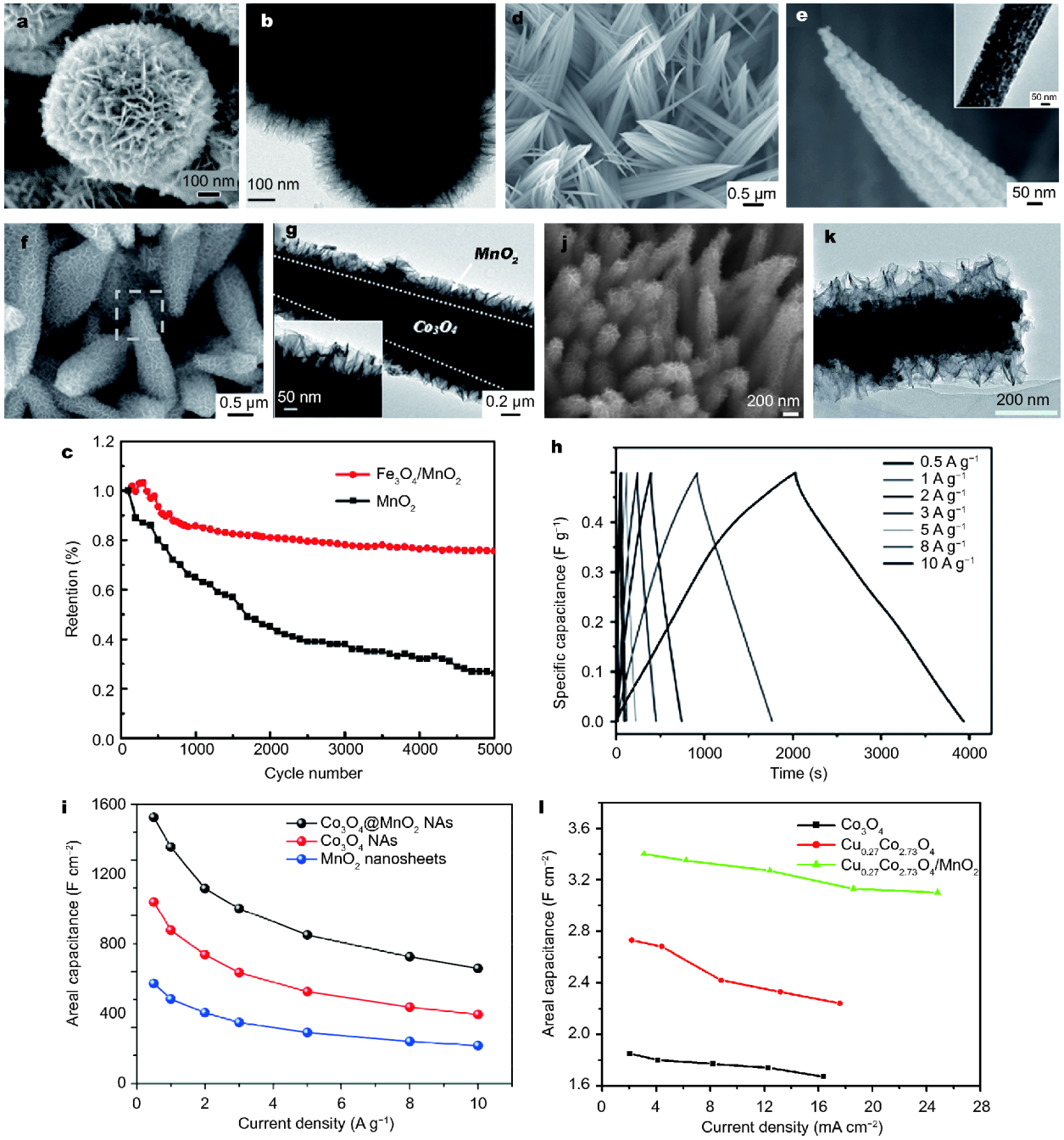

Figure 9 (a) SEM and (b) TEM images of the Fe_3O_4–MnO_2 sample; (c) capacitance retention at 5 A g^{-1} over 5,000 cycles; (d, e) SEM images of the Co_3O_4 NAs (the inset shows TEM image of the Co_3O_4 NAs); (f, g) SEM and TEM images of Co_3O_4@MnO_2 NAs. (h) Charge–discharge curves of the Co_3O_4@MnO_2 composite. (i) Current density dependence of the specific capacitance of the MnO_2 nanosheets, Co_3O_4 NAs and Co_3O_4@MnO_2 NAs. (j, k) SEM and TEM images of $Cu_{0.27}Co_{2.73}O_4$/MnO_2; (l) the specific capacitances of the three electrodes as a function of current density. (a–c) Reproduced with permission from Ref. [137]. Copyright 2014, the American Chemical Society. (d–i) Reproduced with permission from Ref. [138]. Copyright 2014, Wiley-VCH. (j–l) Reproduced with permission from Ref. [139]. Copyright 2015, the Royal Society of Chemistry.

Na_2SO_4). The capacitance retention of the Fe_3O_4–MnO_2 composite is markedly superior to that of single MnO_2 (Fig. 9c). The good electrochemical performance of the Fe_3O_4–MnO_2 sample is attributed to its unique hierarchical nanostructure, in which high-number-density and isolated Fe_3O_4 NPs are distributed in the interior of

MnO_2.

Cheng *et al.* [138] fabricated a hierarchical porous Co_3O_4@MnO_2 nanoneedle arrays (Co_3O_4@MnO_2 NAs) on Ni foam *via* a hydrothermal method. The synthesis of Co_3O_4@MnO_2 NAs can be divided into four steps. First, through a modified hydrothermal process, $Co(OH)_2CO_3$ is directly grown on Ni foam substrate. Further heat treatment enables the formation of porous Co_3O_4 nanostructures. Afterward, the porous Co_3O_4 nanoneedles are coated with a thin carbon nanolayer. Finally, the Co_3O_4@MnO_2 NAs are obtained *via* the formation of MnO_2 nanosheets through a reaction between $KMnO_4$ and carbon. As shown in Fig. 9d, the Co_3O_4 nanoneedles stand on the Ni foam substrate. Each nanoneedle consists of numerous small NPs accumulating with each other, forming a nanoporous structure (shown in Fig. 9e). Fig. 9f, g show the SEM and TEM images of Co_3O_4@MnO_2 NAs. Thin MnO_2 nanosheets are covered on the surface of Co_3O_4 nanoneedles, forming a core-shell hierarchical nanostructure. The galvanostatic charge–discharge curves of the Co_3O_4@MnO_2 NAs investigated at 0.5–10 A g^{-1} (1 mol L^{-1} LiOH) are shown in Fig. 9h. The sample displays relatively high specific capacitances of 1905.4, 1693.2, 1396, 1253.4, 1062, 905.6, and 823 F g^{-1} at 0.5, 1, 2, 3, 5, 8, and 10 A g^{-1}, respectively. Fig. 9i shows that the performance of the Co_3O_4@MnO_2 NAs is obviously better than those of the individual MnO_2 nanosheets and Co_3O_4 nanoneedles. Furthermore, the Co_3O_4@MnO_2 composite materials possess a high energy density of 66.2 W h kg^{-1} at a power density of 0.25 kW kg^{-1}.

A hydrothermal and post-heat treatment method was employed by Yin *et al.* [139] for the preparation of hierarchical $Cu_{0.27}Co_{2.73}O_4$/MnO_2 nanorod arrays. The MnO_2 nanoflakes homogeneously grow on $Cu_{0.27}Co_{2.73}O_4$ nanorods which are grown on Ni foam, and the average diameter of the composites is approximately 250–300 nm (shown in Fig. 9j, k). The specific capacitances of $Cu_{0.27}Co_{2.73}O_4$ and $Cu_{0.27}Co_{2.73}O_4$/MnO_2 are 2.24 F cm^{-2} at 17.6 mA cm^{-2} and 3.1 F cm^{-2} at 24.8 mA cm^{-2}, respectively (Fig. 9l). The specific capacitance of Co_3O_4 at 16.4 mA cm^{-2} is 1.67 F cm^{-2}, which is markedly lower than those of $Cu_{0.27}Co_{2.73}O_4$ and $Cu_{0.27}Co_{2.73}O_4$/MnO_2 electrodes. As the current density increases from 2.2 to 17.6 mA cm^{-2}, the capacity of $Cu_{0.27}Co_{2.73}O_4$ remains at ~82.1%. For $Cu_{0.27}Co_{2.73}O_4$/MnO_2, a better rate capability with approximately 91.2% capacitance retention can be observed as the current density increases from 3.1 to 24.8 mA cm^{-2}. The homogeneously aligned structure of $Cu_{0.27}Co_{2.73}O_4$ nanorods with planar tips and a rough surface can effectively control the aggregation of active materials and shorten the pathway for ion transportation, further resulting in large areal capacitance and superior rate capability. These results demonstrate the opportunity of the potential candidate as binder-free electrodes applied in SCs and show great potential in exploring higher areal capacitance for miniaturized devices.

Liu *et al.* [140] prepared hierarchical $NiCo_2O_4$@MnO_2 core–shell nanosheet array composites on Ni foam by a two-step hydrothermal method. Owing to the unique nanoarchitecture, the $NiCo_2O_4$@MnO_2 core–shell nanosheet arrays display a high areal capacitance of 2.39 F cm^{-2}, (1595.1 F g^{-1}) at 3 mA cm^{-2} (1 mol L^{-1} NaOH). However, the areal capacitance of pure $NiCo_2O_4$ nanosheet arrays was calculated to be only 1.50 F cm^{-2} at 3 mA cm^{-2}. The $NiCo_2O_4$@MnO_2 sample also exhibits good cycle performance (92.6% retention after 2000 cycles at 40 mA cm^{-2}), which is superior to that of the pristine $NiCo_2O_4$ nanosheet sample. The results show that the growth of MnO_2 nanosheets on $NiCo_2O_4$ nanosheets is a viable approach to increase the capacitive properties of materials and simultaneously improve the cycling performance of SCs.

By a facile two-step electro-deposition process, Zhang *et al.* [141] successfully synthesized a 3D hierarchical $NiCo_2O_4$@MnO_2 hybrid nanomaterial grown on stainless steel mesh. The specific capacitance of $NiCo_2O_4$@MnO_2 at 2 A g^{-1} is 688.4 F g^{-1}, which is markedly higher than those of MnO_2 (336.6 F g^{-1}) and $NiCo_2O_4$ (241 F g^{-1}). The $NiCo_2O_4$@MnO_2 shows a high specific capacitance of 913.6 F g^{-1} at 0.5 A g^{-1} and a capacitance retention of 87.1% after 3,000 cycles. Furthermore, the asymmetric SCs device with a large voltage window of 1.5 V is assembled by using $NiCo_2O_4$@MnO_2 sample as the cathode and activated carbon as the anode. The device achieves an energy density of 37.5 W h kg^{-2} at a power density of 187.5 W kg^{-1}.

Composites of gold NP-doped TMOs

TMOs doped with Au NPs are highly active and function as selective catalysts for a variety of chemical reactions [142,143]. The design of the TMOs composites with Au nanoparticles is demonstrated to be another efficient approach to enhance the electrochemical performance of TMOs as SC electrodes [144]. Wang *et al.* [145] designed and synthesized an Au–NiO composite that exhibited a markedly improved rate performance on SCs. The specific capacitance of the Au–NiO electrode at 20 A g^{-1} is 619 F g^{-1}, which is markedly higher than that of pure NiO electrode (216 F g^{-1}).

You *et al.* [146] successfully synthesized mono-

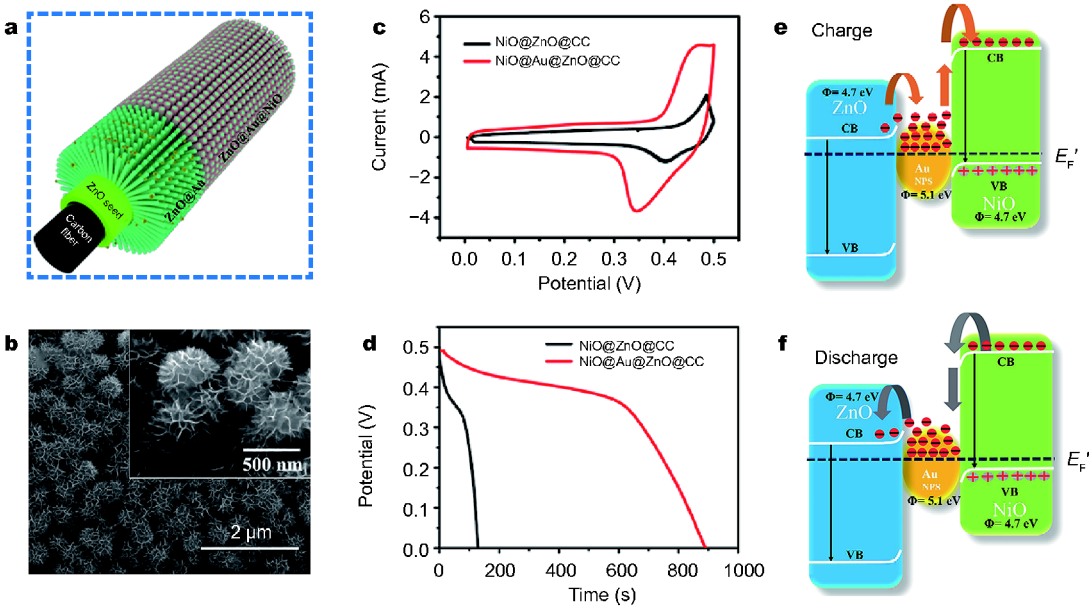

Figure 10 (a) Schematic illustration for the fabrication of hierarchical ZnO@Au@NiO nanocomposite; (b) SEM images of ZnO@Au@NiO; (c) CV curves of two samples; (d) discharge curves of two samples; (e and f) energy level diagrams at the interface of ZnO–Au–NiO during charge–discharge process. Reproduced with permission from Ref. [151]. Copyright 2015, the American Chemical Society.

dispersed dumbbell-like Au–Fe_3O_4 NPs with different sizes (5/14, 5/21, 7/14, and 7/21 nm Au–Fe_3O_4 NPs). The specific capacitance of 7/14 nm Au–Fe_3O_4 NPs at 1 A g^{-1} is 464 F g^{-1} (1 mol L^{-1} KOH), which is markedly higher than that of pure Fe_3O_4 NPs (160 F g^{-1}). The 7/14 nm Au–Fe_3O_4 composite exhibits a higher capacitance retention of 86.4% after 1,000 cycles at 10 A g^{-1} than that of pure Fe_3O_4 NP electrode (72.8% retention of initial capacitance). The above capacitive enhancement can be ascribed to the electron transfer increase induced by gold across the dumbbell-like NPs.

A simple and controllable electrochemical deposition process was employed by Hu's groups to synthesize the 3D hierarchical heterostructure of MnO_2 nanosheets and nanorods directly grown on porous Au-coated Co_3O_4 nanowall array, and to assemble a sandwich construction of Co_3O_4@Au@MnO_2 [147]. Owing to the unique sandwich construction, each component is efficiently used for energy reaction. The specific capacitance of the Co_3O_4@Au@MnO_2 nanosheet hierarchical heterostructures (Co_3O_4@Au@MnO_2 (NSs) HHs) is 1532.4 F g^{-1} at 1 A g^{-1} (1 mol L^{-1} LiOH), which is higher than those of the Au-coated Co_3O_4 nanowall arrays (1046.6 F g^{-1}) and Co_3O_4@Au@MnO_2 nanorod hierarchical heterostructures (Co_3O_4@Au@MnO_2 (NRs) HHs) (1292.9 F g^{-1}). The Co_3O_4@Au@MnO_2 (NSs) HHs also exhibit superior cycling performance (with virtually no degradation after 5,000 cycles). Furthermore, the presented results of the Co_3O_4@Au@MnO_2 (NSs) HHs are larger than those of the reported Co_3O_4 or MnO_2-based heterostructures, such as MnO_2/Mn/MnO_2 nanotube arrays (937 F g^{-1} at 1.5 A g^{-1}) [148], Zn_2SO_4@MnO_2 nanorods (642.3 F g^{-1} at 1 A g^{-1}) [149], and Co_3O_4/NiO nanowire arrays (853 F g^{-1} at 2 A g^{-1}) [150]. Thus, the Co_3O_4@Au@MnO_2 (NSs) HHs could be recognized as promising materials for SCs.

Yan *et al.* [151] designed and synthesized a hierarchical ZnO@Au@NiO nanocomposite as the electrode of SCs (Fig. 10a,b). First, ZnO nanowires arrays were grown on carbon nanofibers of carbon cloth. Then, a small quantity of Au nanoparticles was covered on ZnO nanowires. Subsequently, NiO nanosheets were uniformly grown on the surface of the Au-modified ZnO nanowires to obtain the ZnO@Au@NiO composites. The ZnO/Au/NiO electrode possesses a larger area in the CV curve, suggesting superior electrochemical performance to that of ZnO/NiO nanorods (shown in Fig. 10c). The areal capacitance of the ZnO@Au@NiO nanocomposite is calculated to be 3.50 F cm^{-2} at 2 mA cm^{-2} (1 mol L^{-1} KOH), whereas the ZnO@NiO electrode only shows an areal capacitance of 0.42 F cm^{-2} under the same condition (Fig. 10d). The ZnO@Au@NiO nanocomposite electrode demonstrates good cyclic stability with approximately 80.3% capacitance retention after 4,000 continuous cycles at 30 mA cm^{-2}. The enhanced electrochemical property is

mainly ascribed to the decoration of Au nanoparticles. On one hand, Au nanoparticles can accelerate electron conduction. On the other hand, electrons can be temporarily trapped and accumulated at the Fermi level (E_F) due to the localized Schottky barrier at Au/NiO interface during charge process until filling the gap between ZnO and NiO (Fig. 10e) [151]. Thus, more electrons can be released during discharge process (Fig. 10f).

Composites of carbon materials and TMOs

For pseudocapacitors, surface oxidation–reduction reaction of metal oxides can result in higher specific capacitances [152]. Nanostructured carbon materials are generally utilized as EDLC electrodes, demonstrating their superior long-term electrochemical stability [153]. Thus, considerable efforts have been made to enhance the SC performance by creating composites of TMOs and carbon materials, such as TMOs/graphene and TMOs/carbon nanofibers (CFs) [154–167]. The synthesized multi-component composites can maximize the benefits from all components [154–169].

Wang *et al.* [170] designed and fabricated two types of hierarchical core–shell fiber-based electrodes, including MnO_2/reduced graphene oxide (RGO)/CF and 3D porous graphene hydrogel-wrapped Cu wire (GH/CW). The specific areal capacitance and volumetric capacitance of the MnO_2/RGO/CF electrode are 205.7 mF cm^{-2} and 13.7 F cm^{-3} at 0.5 mA cm^{-2} (1 mol L^{-1} Na_2SO_4), respectively, and both values are considerably larger than those of MnO_2/CF (178.3 mF cm^{-2} and 11.8 F cm^{-3}) and RGO/CF (1.6 mF cm^{-3} and 0.1 F cm^{-3}). The results indicate that the synergistic effect and the interactions between the RGO nanosheets and MnO_2 nanoflakes in the MnO_2/RGO/CF electrode markedly increase the total capacitive performance. The specific capacitance of the MnO_2/RGO/CF electrode remains at 73% from 13.7 to 10 F cm^{-3}. Owing to the synergistic effects of different components in nanohybrid fiber electrodes, the asymmetric SC device with MnO_2/graphene/CF as the cathode and GH/CW as the anode shows a high areal energy density of 18.1 μW h cm^{-2} and a volumetric energy density of 0.9 mW h cm^{-3} in a voltage range of 0–1.6 V. Moreover, the asymmetric SC also shows an energy density as high as 0.63 mW h cm^{-3} at a high power density of 0.2 W cm^{-3}. Thus, the fiber-based flexible SCs show excellent flexibility, great rate capability, and good cycle stability, making these SCs a prospective power source for flexible energy storage devices.

Yu *et al.* [171] fabricated hierarchical graphene/MnO_2 nanostructured sponges by a low-cost "dip and dry" process with commercial sponges as skeletons. The composite can be operated at a high scan rate of 200 V s^{-1} and has superior cycle performance (~90% retention after 10,000 cycles at 10 A g^{-1}). As calculated using galvanostatic charge–discharge curves, the highest energy density and power density of sponge@RGO@MnO_2 based device are 8.34 W h kg^{-1} and 47 kW kg^{-1}, respectively, at an operating voltage of 0.8 V. However, the highest energy density and power density are 2.08 W h kg^{-1} and 94 kW kg^{-1} for the sponge@RGO under the same condition. The features of low cost, facile preparation, wide operation range, high specific capacitance, high energy and power density, and superior cycling performance could make the as-fabricated SCs as promising devices for commercial production.

Kumar *et al.* [172] reported an interesting work about the fabrication of 3D hierarchical structure composed of 0D Co_3O_4 nanobeads, 1D carbon nanotubes (CNTs), and 2D graphenes (GNSs) *via* an easy ultrafast microwave irradiation method for high performance supercapacitor electrode. In this unique structure, Co_3O_4 nanobeads are anchored on CNTs and the CNTs are grown on GNSs, leading to a good electrochemical performance. The electrode possesses a large specific capacitance of 600 F g^{-1} at 0.7 A g^{-1} (30 wt.% KOH). Furthermore, the electrode also exhibits good cycle stability (94.5% retention after 5,000 cycles at 10 A g^{-1}).

Flexible solid-state fiber SCs present the advantages of light weight, high power density, good flexibility, low cost, and environmental friendliness. Zhang *et al.* [173] fabricated a MnO_2/CFs fiber *via* electrodepositing ultrathin MnO_2 nanosheets on carbon fiber yarns. The specific volumetric and gravimetric capacitances of the single MnO_2/CFs fiber electrode are calculated to be 58.7 F cm^{-3} and 428 F g^{-1} based on the mass of MnO_2. The MnO_2/CFs electrode demonstrates a large volumetric capacitance because of the synergistic effects of MnO_2 and CFs. The assembled flexible solid-state fiber-like SCs (two MnO_2/CFs fiber electrodes as anode and cathode, resepectively) show a high volumetric energy density (3.8 mW h cm^{-3} at a power density of 89 mW cm^{-3}), superior flexibility (CV curves are almost unaltered after 2,000 bending times), and an excellent cycling performance (only 14.2% capacitance fade after 10,000 cycles).

By a hydrothermal method, Hu *et al.* [174] fabricated a hierarchical mesoporous $NiFe_2O_4$ (NFO) nanocone forest that directly grew on carbon textile (CT). In the NFO–CT sample, the compact bundle of fibers possesses an average diameter of approximately 5 μm. The BET specific surface area of the hierarchical NFO–CT is as

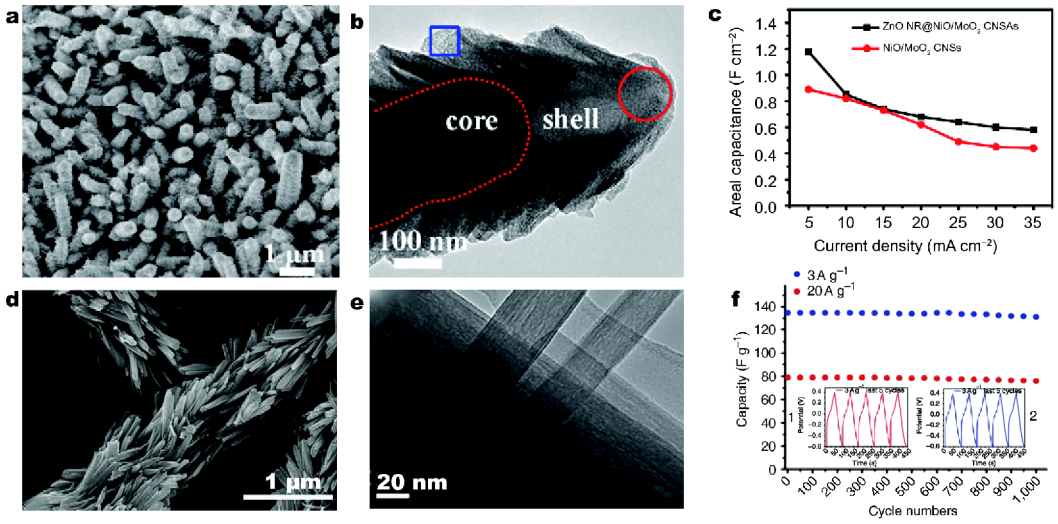

Figure 11 (a) SEM and (b) TEM images of ZnO NR@NiO/MoO_2 CNSAs; (c) the areal specific capacitances of the two electrodes as a function of current density; (d) SEM image of $MnMoO_4$/$CoMoO_4$ heterostructured nanowires; (e) TEM image at the heterojunction of the hierarchical $MnMoO_4$/$CoMoO_4$ heterostructured nanowires; (f) cycling performance of $MnMoO_4$/$CoMoO_4$ (3D) electrodes tested at 3 and 20 A g^{-1} (the inset shows charge–discharge curves cycled at the first and last five cycles at 3 A g^{-1}). (a–c) Reproduced with permission from Ref. [176]. Copyright 2014, the American Chemical Society. (d–f) Reproduced with permission from Ref. [177]. Copyright 2011, Nature Publishing Group.

high as 593.60 m^2 g^{-1}. As a binder-free electrode, the NFO–CT exhibits specific capacitances of 697, 543.5, 421.8, 355.2, and 303 F g^{-1} at 5, 10, 25, 50, and 75 mV s^{-1} (6 mol L^{-1} LiCl), respectively. Furthermore, the symmetric solid-state SCs device based on NFO–CT demonstrates high capacitance (584 F g^{-1} at 5 mV s^{-1}) and excellent cycle performance (93.57% capacitance retention after 10,000 cycles). The energy density is calculated to be 54.9 W h kg^{-1} at a power density of 300 W kg^{-1}. Even at 1372 W kg^{-1}, the NFO–CT electrode still achieves an energy density of 25.5 W h kg^{-1}, which is substantially higher than those of single/binary metal oxide-based electrodes.

An easy, low-cost, and controllable approach was used by Zhang *et al.* [175] for the synthesis of corrugated $NiCo_2O_4$ nanosheets on a nitrogen-doped graphene/carbon nanotube (NGN/CNT) film. The $NiCo_2O_4$/NGN/CNT film electrode possesses a high volumetric capacitance of 482.7 F cm^{-3} and a gravimetric capacitance of 2292.7 F g^{-1} at 5 A g^{-1} (6 mol L^{-1} KOH). The electrode also exhibits high rate capability and extremely long-term cycle stability. The asymmetric SCs device was fabricated by using $NiCo_2O_4$/NGN/CNTs as the cathode and NGN/CNTs as the anode. The device exhibits a high gravimetric energy density of 42.71 W h kg^{-1} at 775 W kg^{-1} and a high gravimetric power density of 15485 W kg^{-1} at 24.69 W h kg^{-1}. Thus, this material is better than commercially available $Ni(OH)_2$ used in Ni-MH battery on power density.

Other forms of TMOs composites

Via a two-step solution-based approach, Duan *et al.* [176] synthesized a hierarchical core–shell structure of ZnO nanorod@NiO/MoO_2 composite nanosheet arrays (ZnO NR@NiO/MoO_2 CNSAs) on a Ni foam substrate. As shown in Fig. 11a, the ZnO NR@NiO/MoO_2 CNSAs possess a diameter of ~600 nm and length of ~4 μm. The nanorod consists of a ZnO NR "core" and a NiO/MoO_2 CNS "shell", and the ZnO NRs are well wrapped with ultrathin NiO/MoO_2 CNSs (shown in Fig. 11b). The unique structure favors the penetration of electrolytes into the interior of the active material. The areal specific capacitance of the ZnO NR@NiO/MoO_2 CNSAs is 1.18 F cm^{-2} at 5 mA cm^{-2} (2 mol L^{-1} KOH) (shown in Fig. 11c). Moreover, the material also shows a good cycling performance (only 8.3% loss after 4,000 cycles at 10 mA cm^{-2}).

Mai *et al.* [177] synthesized a 3D hierarchical $MnMoO_4$/$CoMoO_4$ heterostructure by a refluxing approach under mild conditions and $MnMoO_4$ as the backbone material. Fig. 11d shows the morphology and structure of the $MnMoO_4$/$CoMoO_4$ hierarchical heterostructure. The pure $MnMoO_4$ nanowire backbone materials are approximately 10 μm in length and 500 nm in

diameter. Furthermore, as shown in Fig. 11e, the $CoMoO_4$ nanorods with diameters of around 50 nm are obtained. The BET specific surface areas of $MnMoO_4$, $MnMoO_4$/$CoMoO_4$ nanocomposite, and surface-modified $MnMoO_4$/$CoMoO_4$ are 3.17, 28.0, and 54.06 $m^2 g^{-1}$, respectively. The active sites of the electrode can be adequately accessed due to the larger surface area compared with that in a previous report [178] (15 and 25 $m^2 g^{-1}$, which correspond to $MnMoO_4$ nanorods and $CoMoO_4$ nanorods, respectively). The specific capacitances of the hierarchical $MnMoO_4$/$CoMoO_4$ heterostructured nanowires is 187.1 F g^{-1} at 1 A g^{-1} (2 mol L^{-1} NaOH), which is evidently higher than those of pure 1D nanorod $MnMoO_4$ (9.7 F g^{-1}), $CoMoO_4$ (62.8 F g^{-1}), and the $MnMoO_4$/$CoMoO_4$ nanocomposite (69.2 F g^{-1}). Fig. 11f displays excellent reversibility of the hierarchical $MnMoO_4$/$CoMoO_4$ electrode with high cycling efficiency of up to 98% after 1,000 cycles.

Through a stepwise hydrothermal method, Mai *et al.* [179] designed and synthesized 3D self-supported Co_3O_4@$CoMoO_4$ core–shell architectures that directly grew on Ni foam. The Co_3O_4@$CoMoO_4$ shows a high capacitance of 1902 F g^{-1} at 1 A g^{-1} and good cycling stability with 1% capacitance loss after 5,000 cycles at 5 A g^{-1} (2 mol L^{-1} KOH). The asymmetric SCs device was fabricated by using Co_3O_4@$CoMoO_4$ as the cathode and the CNTs on Ni foam as the anode. The device delivers a high energy density of 45.2 W h kg^{-1} at a power density of 400 W kg^{-1} and good cycling performance (capacitance retention of 98.5% after 3,000 cycles at 0.5 A g^{-1}). The good electrochemical performance of Co_3O_4@$CoMoO_4$ is ascribed to the unique architecture with a large interfacial area and numerous channels for the rapid diffusion of electrolyte ions.

High areal specific capacitance per area is of great importance for the practical application of supercapacitors. To realize this goal, it need to combine high mass-loading of the active material and high utilization ratio of the material. Sun *et al.* [180] prepared a ternary hierarchical core-shell structure of Co_3O_4@Ni–Co–O arrays *via* an easy and cost-effective strategy (Fig. 12a–c). As shown in Fig. 12a, the Co_3O_4 microsheet grown on foam Ni substrate is the core, and the aligned slim Ni–Co–O nanorods (diameter <20 nm) are coated on it. This structure exhibits an excellent electrochemical performance when utilized as a supercapacitor electrode. The electrode with a high areal mass-loading of 12 mg cm^{-2} possesses a high specific capacitance of 2098 F g^{-1} at 5 mA cm^{-2} (1 mol L^{-1} KOH) (Fig. 12d). Furthermore, Sun *et al.* [181] also fabricated a hierarchical core-shell structure of Co_3O_4@NiO nanowire@nanorod arrays *via* a similar strategy (Fig. 12e). The NiO nanorods were *in-situ* grown on the surface of Co_3O_4 nanowire arrays grown on foam Ni substrate (Fig. 12f–i). The electrode with a high mass-loading of 19.5 mg cm^{-1} delivers a high specific capacitance of 2033 F g^{-1} at 5 mA cm^{-2} (1 mol L^{-1} KOH). The areal capacitance is up to 39.6 F cm^{-2}, which is much higher than that of pure Co_3O_4 electrode (6.7 F cm^{-2}) (Fig. 12j, k). The excellent performance of these core-shell structure arrays is mainly attributed to the special hierarchical structure and the synergistic effect of different components. Based on the above two works, Sun *et al.* [182] further prepared hierarchical $Co_xFe_{3-x}O_4$ arrays directly grown on Cu foam. Combining the above hierarchical Co_3O_4@Ni–Co–O arrays as the cathode, an aqueous battery was assembled. The battery shows an energy density of ~2.08 mW h cm^{-2} at a power density of ~4.89 mW cm^{-2}, and an energy density of ~1.36 mW h cm^{-2} at a power density of ~42.56 mW cm^{-2} (6 mol L^{-1} KOH). This indicates that hierarchically nanostructured metal oxides also have potential applications in the field of aqueous battery [182].

Iron oxides have been considered to be promising anode materials for supercapacitors due to their low cost, abundance, non-toxicity, and functionality in negative potentials [183–185]. Recently, Lin and co-workers [183] prepared a hierarchical Fe_2O_3 nanotube array directly grown on Ni foam *via* chemical transformation of ZnO nanowire. The characterization results show that the walls of nanotube are mainly composed of α-Fe_2O_3 nanoparticles mixed with a small quantity of ZnO nanoparticles. The electrochemical test results indicate that the hierarchical structure electrode exhibits a high reversible capacitance of 300.1 F g^{-1} at 0.75 A g^{-1} (1 mol L^{-1} Li_2SO_4).

A comparison of typical hierarchically nanostructured TMOs for SCs is given in Table 1. The morphologies and structures of TMOs are important influential factors for the corresponding electrochemical performance. Moreover, the performance of the reported asymmetric supercapacitors is summarized in Table 2.

CONCLUSIONS AND OUTLOOKS

In this review, we summarized the recent progress in the field of hierarchically nanostructured TMOs for SCs. Hierarchically nanostructured TMOs with various structures and compositions have been fabricated *via* different synthesis methods. The primary structure mainly includes spheres, hollow spheres, rods, and tubes at micrometer scale or sub-micrometer scale. The secondary structure is mainly a 2D nanosheet, which is not only

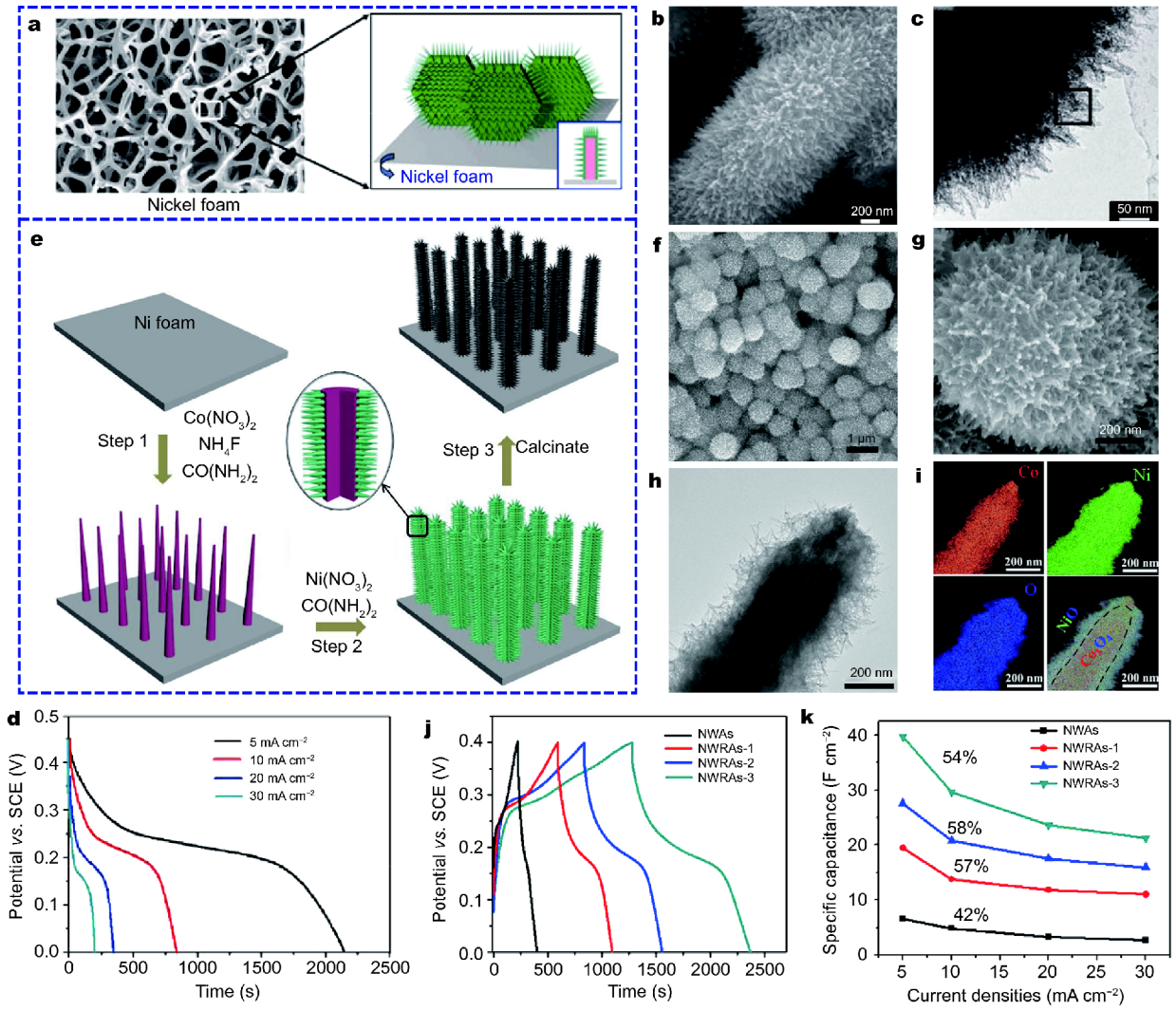

Figure 12 (a) Schematic image for the design of hierarchical core-shell Co_3O_4@Ni–Co–O nanoarray (the Co_3O_4 nanosheet is shown in pink and the Ni–Co–O nanorod is shown in green); (b, c) SEM and TEM images of the hierarchical Co_3O_4@Ni–Co–O arrays; (d) galvanostatic discharge curves of the hierarchical Co_3O_4@Ni–Co–O arrays at various current densities; (e) schematic image for the design of hierarchical core-shell Co_3O_4@NiO arrays (in this work, three samples were fabricated by adding 1, 2, and 3 mmol $Ni(NO_3)_2{\cdot}6H_2O$ during the synthesis process. These three samples were denoted as NWRAs-1, NWRAs-2, and NWRAs-3, respectively. Co_3O_4 nanowire arrays sample was denoted as NWAs); (f, g) SEM images of NWRAs-3 at different magnifications; (h, i) TEM and EDS mapping images of NWRAs-3; (j) galvanostatic charge and discharge curves at 10 mA cm^{-2}; (k) plots of areal specific capacitance *versus* current density. (a–d) Reproduced with permission from Ref. [180]. Copyright 2012, Springer. (e–k) Reproduced with permission from Ref. [181]. Copyright 2014, Elsevier.

beneficial to the stability of the hierarchical structure but also conducive to electrochemical reaction. Single-metal oxides, bimetallic oxides, the composites of different metal oxides, and the composites of metal oxides with carbon nanomaterials or noble metal NPs have been studied extensively for the compositions of hierarchically nanostructured TMOs. In general, bimetallic oxides or composites with different metal oxides exhibit higher electrochemical activities compared with single-metal oxides because of the complex chemical compositions and the synergetic effect of the individual components.

For further improvement in the performance of SCs, the development of new types of hierarchically nanostructured TMO materials would become the focus of future research. The details can be listed as follows:

(1) The incorporation of TMO materials with various nanostructured carbon materials, such as CNTs, CFs, and graphene, can not only inherit the 1D or 2D structures of these carbon materials but also can effectively improve the electrical conductivity of the TMOs. The synthesized

Table 1 Comparison of typical hierarchically nanostructured TMOs as electrodes of SCs in three-electrode systems

Materials	SSA[a] (m^2 g^{-1})	Electrolyte	Capacitance/current density	Retention (%)/cycles/current density	Ref.
Flower-like α-MnO_2	216	1 mol L^{-1} K_2SO_4	298 F g^{-1} /0.117 A g^{-1}	90/2000/2 A g^{-1}	[76]
α-MnO_2 microspheres	/	1 mol L^{-1} Na_2SO_4	365 F g^{-1} /2 A g^{-1}	100/2000/2 A g^{-1}	[77]
β-MnO_2 nanoflowers	267	1 mol L^{-1} Na_2SO_4	296.3 F g^{-1} /2 mV s^{-1}	/	[78]
MnO_2 NFs[b]	269	1 mol L^{-1} Na_2SO_4	176 F g^{-1} /20 A g^{-1}	100/2000/2 A g^{-1}	[79]
δ-MnO_2 microspheres	238	1 mol L^{-1} Na_2SO_4	364 F g^{-1} /1 A g^{-1}	100/6000/10 A g^{-1}	[80]
Co_3O_4 film	/	2 mol L^{-1} KOH	352 F g^{-1} /2 A g^{-1}	/	[91]
Enoki mushroom-like Co_3O_4	/	6 mol L^{-1} KOH	787 F g^{-1} /1 A g^{-1}	94.5/1000/10 A g^{-1}	[92]
HFC Co_3O_4[c]	245.5	2 mol L^{-1} KOH	948.9 F g^{-1} /1 A g^{-1}	/	[93]
NiO NWs[d]	/	6 mol L^{-1} KOH	1493 F g^{-1} /3 A g^{-1}	87/2000/50 mV s^{-1}	[100]
NiO NTAs[e]	165	1 mol L^{-1} Na_2SO_4	675 F g^{-1} /2 A g^{-1}	93.2/10000/2 A g^{-1}	[101]
D–NiO[f]	92.99	2 mol L^{-1} KOH	612.5 F g^{-1} /0.5 A g^{-1}	90/1000/0.5 A g^{-1}	[102]
NiO–HMNAs[g]	312.6	2 mol L^{-1} KOH	3114 F g^{-1} /5 mA cm^{-2}	87.6/4000/30 mA cm^{-2}	[103]
CNRNP[h]	/	3 mol L^{-1} KOH	800 F g^{-1} /200 mV s^{-1}	/	[106]
Flower-like CuO	/	5 mol L^{-1}NaOH	1641 mF cm^{-2} /2 mA cm^{-2}	79/10000/4 mA cm^{-2}	[107]
Flower-shaped CuO	119.6	1 mol L^{-1} KOH	520 F g^{-1} /1 A g^{-1}	95.2/5000/1 A g^{-1}	[108]
Bi_2O_3 NBs[i]	196	1 mol L^{-1} Na_2SO_4	250 F g^{-1} /100 mV s^{-1}	100/1000/100 mV s^{-1}	[113]
Rod-like Bi_2O_3	/	6 mol L^{-1} KOH	1350 F g^{-1} /0.1 A g^{-1}	97.6/1000/0.1 A g^{-1}	[114]
$NiCo_2O_4$ microspheres	148.5	6 mol L^{-1} KOH	1006 F g^{-1} /1 A g^{-1}	93.2/1000/8 A g^{-1}	[124]
$NiCo_2O_4$ MHSs[j]	118.3	3 mol L^{-1} KOH	2623 F g^{-1} /1 A g^{-1}	99.2/3000/10 A g^{-1}	[125]
$NiCoO_2$ NTs[k]	98.9	2 mol L^{-1} KOH	1468 F g^{-1} /2 A g^{-1}	99.2/3000/10 A g^{-1}	[126]
ZnV_2O_4 NHNs[l]	/	2 mol L^{-1} KOH	385 F g^{-1} /0.5 A g^{-1}	89/1000/1 A g^{-1}	[127]
CoO@MnO_2 core-shell	154.95	6 mol L^{-1} KOH	1835 F g^{-1} /1 A g^{-1}	97.7/10000/1 A g^{-1}	[136]
Fe_3O_4–MnO_2 microspheres	/	1 mol L^{-1} Na_2SO_4	367.4 F g^{-1} /100 mV s^{-1}	76/5000/5 A g^{-1}	[137]
Co_3O_4@MnO_2 NAs[m]	/	1 mol L^{-1} LiOH	1905.4 F g^{-1} /0.5 A g^{-1}	89.8/5000/2 A g^{-1}	[138]
$Cu_{0.27}Co_{2.73}O_4$/MnO_2 NRAs[n]	/	6 mol L^{-1} KOH	3.1 F cm^{-2} /24.8 mA cm^{-2}	/	[139]
$NiCo_2O_4$@MnO_2 core-shell	75.06	1 mol L^{-1} NaOH	1595.1 F g^{-1} /3 mA cm^{-2}	92.6/2000/40 mA cm^{-2}	[140]
$NiCo_2O_4$@MnO_2 nanosheets	/	1 mol L^{-1} KOH	913.6 F g^{-1} /0.5 A g^{-1}	87.1/3000/0.5 A g^{-1}	[141]
Dumbbell-like Au-Fe_3O_4	/	1 mol L^{-1} KOH	464 F g^{-1} /1 A g^{-1}	86.4/1000/10 A g^{-1}	[146]
Co_3O_4@Au@MnO_2(NSs)HHs[o]	/	1 mol L^{-1} LiOH	1532.4 F g^{-1} /1 A g^{-1}	115/5000/10 A g^{-1}	[147]
ZnO@Au@NiO	/	1 mol L^{-1} KOH	3.5 F cm^{-2} /2 mA cm^{-2}	80.3/4000/30 mA cm^{-2}	[151]
MnO_2/RGO/CF[p]	/	1 mol L^{-1} Na_2SO_4	13.7 F cm^{-3} /0.5 mA cm^{-2}	/	[170]
3D Co_3O_4-nb@CG[q]	/	30 wt.% KOH	600.19 F g^{-1} /0.7 A g^{-1}	95.4/5000/1.1 A g^{-1}	[172]
$NiFe_2O_4$-CT[r]	/	6 mol L^{-1} LiCl	697 F g^{-1}/5 mV s^{-1}	/	[174]
$NiCo_2O_4$/NGN/CNTs[s]	/	6 mol L^{-1} KOH	2292.7 F g^{-1}/5 A g^{-1}	125/10000/30 A g^{-1}	[175]
ZnO NR@NiO/MoO_2 CNSAs[t]	/	2 mol L^{-1} KOH	1.18 F cm^{-2}/5 mA cm^{-2}	91.7/4000/10 mA cm^{-2}	[176]
$MnMoO_4$/$CoMoO_4$ nanowires	54.06	2 mol L^{-1} NaOH	187.1 F g^{-1} /1 A g^{-1}	98/1000/20 A g^{-1}	[177]
Co_3O_4@$CoMoO_4$ core–shell	61.4	2 mol L^{-1} KOH	1902 F g^{-1} /1 A g^{-1}	99/5000/5 A g^{-1}	[179]
Co_3O_4@Ni–Co–O NSRAs[u]	31.1	1 mol L^{-1} KOH	2098 F g^{-1}/5 mA cm^{-2}	96/1000/30 mA cm^{-2}	[180]
Co_3O_4@NiO NWRAs[v]	116	1 mol L^{-1} KOH	2033 F g^{-1}/5 mA cm^{-2}	100/1000/30 mA cm^{-2}	[181]
α-Fe_2O_3 nanotubes	/	1 mol L^{-1} Li_2SO_4	300.1 F g^{-1}/0.75 A g^{-1}	/	[183]

a) SSA: specific surface area. b) MnO_2 NFs: MnO_2 nanoflakes; c) HFC Co_3O_4: hollow fluffy cages Co_3O_4; d) NiO NWs: NiO nanowires; e) NiO NTAs: NiO nanotube arrays; f) D–NiO: double-shelled NiO; g) NiO–HMNAs: hierarchical mesoporous NiO nanoarrays; h) CNRNP: CuO nanoribbon-on-Ni-nanoporous/Ni foam; i) Bi_2O_3 NBs: Bi_2O_3 nanobelts; j) $NiCo_2O_4$ MHSs: $NiCo_2O_4$ multiple hierarchical structures; k) $NiCoO_2$ NTs: $NiCoO_2$ nanotube; l) ZnV_2O_4 NHNs: ZnV_2O_4 novel hierarchical nanospheres; m) Co_3O_4@MnO_2 NAs: Co_3O_4@MnO_2 nanoneedle arrays; n) $Cu_{0.27}Co_{2.73}O_4$/MnO_2 NRAs: $Cu_{0.27}Co_{2.73}O_4$/MnO_2 nanorod arrays; o) Co_3O_4@Au@MnO_2 (NSs) HHs: Co_3O_4@Au@MnO_2 nanosheet hierarchical heterostructures; p) MnO_2/RGO/CF: MnO_2/reduced graphene oxide/carbon nanofiber; q) Co_3O_4-nb@CG: Co_3O_4 nanobeads–CNTs (carbon nanotubes)–GNSs (graphene nanosheets). r) $NiFe_2O_4$–CT: $NiFe_2O_4$ nanocone forest on carbon textile; s) $NiCo_2O_4$/NGN/CNTs: $NiCo_2O_4$ nanosheets on nitrogen-doped graphene/carbon nanotubes; t) ZnO NR@NiO/MoO_2 CNSAs: ZnO nanorod@NiO/MoO_2 composite nanosheet arrays; u) Co_3O_4@Ni–Co–O NSRAs: Co_3O_4@Ni–Co–O nanosheet@nanorod arrays; v) Co_3O_4@NiO NWRAs: Co_3O_4@NiO nanowire@nanorod arrays.

Table 2 Typical hierarchically nanostructured TMOs as cathodes of asymmetric SCs

Cathode materials	Anode materials	Working voltage	Device performance[a]		Ref.
			Energy density	Power density	
δ-MnO_2 microspheres	Activated carbon	0–2 V	48.06 W h kg^{-1}	1.0 kW kg^{-1}	[80]
Enoki mushroom-like Co_3O_4	Carbon	0–1.5 V	23.9 W h kg^{-1}	0.375 kW kg^{-1}	[92]
CoO@MnO_2 core-shell	Nitrogen-doped graphene	0–1.8 V	85.9 W h kg^{-1}	852.4 W kg^{-1}	[136]
$NiCo_2O_4$@MnO_2 nanosheets	Activated carbon	0–1.5 V	37.5 W h kg^{-1}	187.5 W kg^{-1}	[141]
MnO_2/RGO/CF[b]	GH/CW[c]	0–1.6 V	0.63 mW h cm^{-3}	0.2 W cm^{-3}	[170]
$NiCo_2O_4$/NGN/CNTs[d]	NGN/CNTs[e]	0–1.55 V	42.7 W h kg^{-1}	775 W kg^{-1}	[175]
Co_3O_4@$CoMoO_4$ core–shell	CNTs[f]	0–1.6 V	45.2 W h kg^{-1}	400 W kg^{-1}	[179]

a) Device performance: the energy density of the asymmetric SCs device under a certain power density. b) MnO_2/RGO/CF: MnO_2/reduced graphene oxide/carbon nanofiber; c) GH/CW: graphene hydrogel-wrapped Cu wire; d) $NiCo_2O_4$/NGN/CNTs: $NiCo_2O_4$ nanosheets on nitrogen-doped graphene/carbon nanotubes; e) NGN/CNTs: nitrogen-doped graphene/carbon nanotubes; f) CNTs: carbon nanotubes.

multi-component composites can maximize the benefits from all components, thereby making this approach a highly effective method to improve the performance of the TMO materials. Despite several reports on the composites of metal oxides with carbon nanomaterials, these materials still present massive development space in the future.

(2) Compared with general nanostructured TMOs, hierarchically nanostructured TMOs exhibits higher specific capacitance and better rate performance. However, although the hierarchical nanostructure is favorable for the electrochemical reaction of TMO electrode materials, this special structure often leads to the low tap density of the materials. Therefore, new reasonable structures should be designed for hierarchically nanostructured TMOs to endure large volume energy densities.

(3) It is obvious that the specific capacitances of most of the cobalt-based materials and nickel-based materials are much larger than those of other materials. Therefore, these materials are promising for practical applications. The future research of TMOs-based electrode materials can be focused on cobalt-based materials and nickel-based materials.

(4) The asymmetric SCs are a hot spot in the SC field at present. For asymmetric SCs, various negative and positive electrode materials with well-separated potential windows can be combined to maximize the output voltage; thus, the specific energy of SCs will be markedly increased.

(5) The self-supporting flexible electrode in SCs is another important research direction. When self-supporting flexible materials are used as electrodes, the conductive carbon and bonding agent are unnecessary for the assembly of SC device; thus, the energy density of device can be effectively improved. In addition, the self-supporting flexible electrode can enhance the circulation stability of device. Furthermore, the flexible all-solid-state asymmetric SCs device is crucial because of several advantageous properties, such as a wide operating voltage range, high energy densities, excellent flexibility, and superior long term cycling stability.

(6) Aqueous rechargeable batteries, such as Ni–Zn battery, Ni–MH battery, and Ni–Fe battery, have attracted renewed interest because of their high theoretical energy density, long cycling life, low cost, and safety [186]. Hierarchically nanostructured TMOs reviewed in this paper also can be applied in aqueous batteries [186]. This is also a very important research direction.

Received 7 July 2017; accepted 10 August 2017; published online 17 October 2017

1 Simon P, Gogotsi Y. Materials for electrochemical capacitors. Nat Mater, 2008, 7: 845–854
2 Wang X, Lu X, Liu B, *et al.* Flexible energy-storage devices: design consideration and recent progress. Adv Mater, 2014, 26: 4763–4782
3 Xie K, Wei B. Materials and structures for stretchable energy storage and conversion devices. Adv Mater, 2014, 26: 3592–3617
4 Yu D, Goh K, Wang H, *et al.* Scalable synthesis of hierarchically structured carbon nanotube–graphene fibres for capacitive energy storage. Nat Nanotech, 2014, 9: 555–562
5 Cheng XB, Huang JQ, Zhang Q, *et al.* Aligned carbon nanotube/sulfur composite cathodes with high sulfur content for lithium–sulfur batteries. Nano Energ, 2014, 4: 65–72
6 Kim MS, Lim E, Kim S, *et al.* General synthesis of N-doped macroporous graphene-encapsulated mesoporous metal oxides and their application as new anode materials for sodium-ion hybrid supercapacitors. Adv Funct Mater, 2017, 27: 1603921
7 Zhang J, Zhao XS. On the configuration of supercapacitors for maximizing electrochemical performance. ChemSusChem, 2012, 5: 818–841
8 Simon P, Gogotsi Y, Dunn B. Where do batteries end and supercapacitors begin? Science, 2014, 343: 1210–1211
9 Lu Z, Wu X, Jiang M, *et al.* Transition metal oxides/hydroxides nanoarrays for aqueous electrochemical energy storage systems. Sci China Mater, 2014, 57: 59–69

10 Feng N, He P, Zhou H. Enabling catalytic oxidation of Li_2O_2at the liquid-solid interface: the evolution of an aprotic Li-O_2 battery. ChemSusChem, 2015, 8: 600–602
11 Peng S, Li L, Hu Y, *et al.* Fabrication of spinel one-dimensional architectures by single-spinneret electrospinning for energy storage applications. ACS Nano, 2015, 9: 1945–1954
12 Jiang J, He P, Tong S, *et al.* Ruthenium functionalized graphene aerogels with hierarchical and three-dimensional porosity as a free-standing cathode for rechargeable lithium-oxygen batteries. NPG Asia Mater, 2016, 8: e239
13 Tong S, Zheng M, Lu Y, *et al.* Mesoporous NiO with a single-crystalline structure utilized as a noble metal-free catalyst for non-aqueous Li–O_2 batteries. J Mater Chem A, 2015, 3: 16177–16182
14 Yang S, He P, Zhou H. Exploring the electrochemical reaction mechanism of carbonate oxidation in Li–air/CO_2 battery through tracing missing oxygen. Energ Environ Sci, 2016, 9: 1650–1654
15 Zhang S, Zheng M, Lin Z, *et al.* Activated carbon with ultrahigh specific surface area synthesized from natural plant material for lithium–sulfur batteries. J Mater Chem A, 2014, 2: 15889–15896
16 Li N, Zheng M, Lu H, *et al.* High-rate lithium–sulfur batteries promoted by reduced graphene oxide coating. Chem Commun, 2012, 48: 4106–4108
17 Zhong Y, Xia X, Shi F, *et al.* Transition metal carbides and nitrides in energy storage and conversion. Adv Sci, 2016, 3: 1500286
18 Xie D, Xia X, Zhong Y, *et al.* Exploring advanced sandwiched arrays by vertical graphene and N-doped carbon for enhanced sodium storage. Adv Energ Mater, 2017, 7: 1601804
19 Wang Y, Song Y, Xia Y. Electrochemical capacitors: mechanism, materials, systems, characterization and applications. Chem Soc Rev, 2016, 45: 5925–5950
20 Wang G, Zhang L, Zhang J. A review of electrode materials for electrochemical supercapacitors. Chem Soc Rev, 2012, 41: 797–828
21 Liu L, Niu Z, Chen J. Unconventional supercapacitors from nanocarbon-based electrode materials to device configurations. Chem Soc Rev, 2016, 45: 4340–4363
22 Chen S, Xing W, Duan J, *et al.* Nanostructured morphology control for efficient supercapacitor electrodes. J Mater Chem A, 2013, 1: 2941–2954
23 Cao X, Yin Z, Zhang H. Three-dimensional graphene materials: preparation, structures and application in supercapacitors. Energ Environ Sci, 2014, 7: 1850–1865
24 Qu C, Jiao Y, Zhao B, *et al.* Nickel-based pillared MOFs for high-performance supercapacitors: design, synthesis and stability study. Nano Energ, 2016, 26: 66–73
25 Dong Y, Xu X, Li S, *et al.* Inhibiting effect of Na^+ pre-intercalation in MoO_3 nanobelts with enhanced electrochemical performance. Nano Energ, 2015, 15: 145–152
26 Zhang LL, Zhao XS. Carbon-based materials as supercapacitor electrodes. Chem Soc Rev, 2009, 38: 2520–2531
27 Naoi K, Naoi W, Aoyagi S, *et al.* New generation "nanohybrid supercapacitor". Acc Chem Res, 2013, 46: 1075–1083
28 Lu X, Yu M, Wang G, *et al.* Flexible solid-state supercapacitors: design, fabrication and applications. Energ Environ Sci, 2014, 7: 2160–2181
29 Li B, Zheng M, Xue H, *et al.* High performance electrochemical capacitor materials focusing on nickel based materials. Inorg Chem Front, 2016, 3: 175–202
30 Zhang F, Liu T, Hou G, *et al.* Hierarchically porous carbon foams for electric double layer capacitors. Nano Res, 2016, 9: 2875–2888
31 Tan Q, Wang P, Liu H, *et al.* Hollow MO_x-RuO_2 (M = Co, Cu, Fe, Ni, CuNi) nanostructures as highly efficient electrodes for supercapacitors. Sci China Mater, 2016, 59: 323–336
32 Nie Z, Wang Y, Zhang Y, *et al.* Multi-shelled α-Fe_2O_3 microspheres for high-rate supercapacitors. Sci China Mater, 2016, 59: 247–253
33 Kumar R, Singh RK, Kumar Dubey P, *et al.* Hydrothermal synthesis of a uniformly dispersed hybrid graphene–TiO_2 nanostructure for optical and enhanced electrochemical applications. RSC Adv, 2015, 5: 7112–7120
34 Kumar R, Singh RK, Vaz AR, *et al.* Microwave-assisted synthesis and deposition of a thin ZnO layer on microwave-exfoliated graphene: optical and electrochemical evaluations. RSC Adv, 2015, 5: 67988–67995
35 Li Z, Ahadi K, Jiang K, *et al.* Freestanding hierarchical porous carbon film derived from hybrid nanocellulose for high-power supercapacitors. Nano Res, 2017, 10: 1847–1860
36 Shi JL, Du WC, Yin YX, *et al.* Hydrothermal reduction of three-dimensional graphene oxide for binder-free flexible supercapacitors. J Mater Chem A, 2014, 2: 10830–10834
37 Zhai T, Wan L, Sun S, *et al.* Phosphate ion functionalized Co_3O_4 ultrathin nanosheets with greatly improved surface reactivity for high performance pseudocapacitors. Adv Mater, 2017, 29: 1604167
38 Yi J, Qing Y, Wu CT, *et al.* Lignocellulose-derived porous phosphorus-doped carbon as advanced electrode for supercapacitors. J Power Sources, 2017, 351: 130–137
39 Yu M, Lin D, Feng H, *et al.* Boosting the energy density of carbon-based aqueous supercapacitors by optimizing the surface charge. Angew Chem Int Ed, 2017, 56: 5454–5459
40 Li Y, Tang F, Wang R, *et al.* Novel dual-ion hybrid supercapacitor based on a $NiCo_2O_4$ nanowire cathode and MoO_2–C nanofilm anode. ACS Appl Mater Interfaces, 2016, 8: 30232–30238
41 Lu X, Zhai T, Zhang X, *et al.* WO_{3-x}@Au@MnO_2 core-shell nanowires on carbon fabric for high-performance flexible supercapacitors. Adv Mater, 2012, 24: 938–944
42 Yan Y, Gu P, Zheng S, *et al.* Facile synthesis of an accordion-like Ni-MOF superstructure for high-performance flexible supercapacitors. J Mater Chem A, 2016, 4: 19078–19085
43 Amali AJ, Sun JK, Xu Q. From assembled metal–organic framework nanoparticles to hierarchically porous carbon for electrochemical energy storage. Chem Commun, 2014, 50: 1519–1522
44 Liang Q, Ye L, Huang ZH, *et al.* A honeycomb-like porous carbon derived from pomelo peel for use in high-performance supercapacitors. Nanoscale, 2014, 6: 13831–13837
45 Sun G, Zhang X, Lin R, *et al.* Weavable, high-performance, solid-state supercapacitors based on hybrid fibers made of sandwiched structure of MWCNT/rGO/MWCNT. Adv Electron Mater, 2016, 2: 1600102
46 Owusu KA, Qu L, Li J, *et al.* Low-crystalline iron oxide hydroxide nanoparticle anode for high-performance supercapacitors. Nat Commun, 2017, 8: 14264
47 Wu ZS, Wang DW, Ren W, *et al.* Anchoring hydrous RuO_2 on graphene sheets for high-performance electrochemical capacitors. Adv Funct Mater, 2010, 20: 3595–3602
48 Jiang J, Li Y, Liu J, *et al.* Recent advances in metal oxide-based electrode architecture design for electrochemical energy storage. Adv Mater, 2012, 24: 5166–5180
49 Cao CY, Guo W, Cui ZM, *et al.* Microwave-assisted gas/liquid

interfacial synthesis of flowerlike NiO hollow nanosphere precursors and their application as supercapacitor electrodes. J Mater Chem, 2011, 21: 3204–3209
50 Endut Z, Hamdi M, Basirun WJ. Pseudocapacitive performance of vertical copper oxide nanoflakes. Thin Solid Films, 2013, 528: 213–216
51 Zhong JH, Wang AL, Li GR, *et al.* Co_3O_4/$Ni(OH)_2$ composite mesoporous nanosheet networks as a promising electrode for supercapacitor applications. J Mater Chem, 2012, 22: 5656–5665
52 Li R, Ren X, Zhang F, *et al.* Synthesis of Fe_3O_4@SnO_2 core–shell nanorod film and its application as a thin-film supercapacitor electrode. Chem Commun, 2012, 48: 5010–5012
53 Li F, Xing Y, Huang M, *et al.* MnO_2 nanostructures with three-dimensional (3D) morphology replicated from diatoms for high-performance supercapacitors. J Mater Chem A, 2015, 3: 7855–7861
54 Vijayakumar S, Nagamuthu S, Muralidharan G. Supercapacitor studies on NiO nanoflakes synthesized through a microwave route. ACS Appl Mater Interfaces, 2013, 5: 2188–2196
55 Wang C, Zhang X, Zhang D, *et al.* Facile and low-cost fabrication of nanostructured $NiCo_2O_4$ spinel with high specific capacitance and excellent cycle stability. Electrochim Acta, 2012, 63: 220–227
56 Wang C, Zhang X, Li C, *et al.* Facile fabrication of nanostructured $NiCo_2O_4$ supported on Ni foam for high performance electrochemical energy storage. RSC Adv, 2015, 5: 80620–80624
57 Liu X, Liu J, Sun X. $NiCo_2O_4$@NiO hybrid arrays with improved electrochemical performance for pseudocapacitors. J Mater Chem A, 2015, 3: 13900–13905
58 Park S, Nam I, Kim GP, *et al.* Hybrid MnO_2 film with agarose gel for enhancing the structural integrity of thin film supercapacitor electrodes. ACS Appl Mater Interfaces, 2013, 5: 9908–9912
59 Yang P, Ding Y, Lin Z, *et al.* Low-cost high-performance solid-state asymmetric supercapacitors based on MnO_2 nanowires and Fe_2O_3 nanotubes. Nano Lett, 2014, 14: 731–736
60 Kai K, Kobayashi Y, Yamada Y, *et al.* Electrochemical characterization of single-layer MnO_2 nanosheets as a high-capacitance pseudocapacitor electrode. J Mater Chem, 2012, 22: 14691–14695
61 Chen LH, Li XY, Rooke JC, *et al.* Hierarchically structured zeolites: synthesis, mass transport properties and applications. J Mater Chem, 2012, 22: 17381–17403
62 Trogadas P, Ramani V, Strasser P, *et al.* Hierarchically structured nanomaterials for electrochemical energy conversion. Angew Chem Int Ed, 2016, 55: 122–148
63 Choi BG, Huh YS, Hong WH, *et al.* Electroactive nanoparticle directed assembly of functionalized graphene nanosheets into hierarchical structures with hybrid compositions for flexible supercapacitors. Nanoscale, 2013, 5: 3976–3981
64 Duay J, Sherrill SA, Gui Z, *et al.* Self-limiting electrodeposition of hierarchical MnO_2 and $M(OH)_2$/MnO_2 nanofibril/nanowires: mechanism and supercapacitor properties. ACS Nano, 2013, 7: 1200–1214
65 Li Y, Fu ZY, Su BL. Hierarchically structured porous materials for energy conversion and storage. Adv Funct Mater, 2012, 22: 4634–4667
66 Yue Y, Liang H. Hierarchical micro-architectures of electrodes for energy storage. J Power Sources, 2015, 284: 435–445
67 Li S, Dong YF, Wang DD, *et al.* Hierarchical nanowires for high-performance electrochemical energy storage. Front Phys, 2014, 9: 303–322
68 Ma Z, Shao G, Fan Y, *et al.* Construction of hierarchical α-MnO_2 nanowires@ultrathin δ-MnO_2 nanosheets core–shell nanostructure with excellent cycling stability for high-power asymmetric supercapacitor electrodes. ACS Appl Mater Interfaces, 2016, 8: 9050–9058
69 Zhang X, Miao W, Li C, *et al.* Microwave-assisted rapid synthesis of birnessite-type MnO_2 nanoparticles for high performance supercapacitor applications. Mater Res Bull, 2015, 71: 111–115
70 Zhang X, Sun X, Zhang H, *et al.* Comparative performance of birnessite-type MnO_2 nanoplates and octahedral molecular sieve (OMS-5) nanobelts of manganese dioxide as electrode materials for supercapacitor application. Electrochim Acta, 2014, 132: 315–322
71 Zhang X, Sun X, Zhang H, *et al.* Microwave-assisted reflux rapid synthesis of MnO_2 nanostructures and their application in supercapacitors. ElectroChim Acta, 2013, 87: 637–644
72 Zhang X, Yu P, Zhang H, *et al.* Rapid hydrothermal synthesis of hierarchical nanostructures assembled from ultrathin birnessite-type MnO_2 nanosheets for supercapacitor applications. Electrochim Acta, 2013, 89: 523–529
73 Yu P, Zhang X, Chen Y, *et al.* Solution-combustion synthesis of ε-MnO_2 for supercapacitors. Mater Lett, 2010, 64: 61–64
74 Yu P, Zhang X, Wang D, *et al.* Shape-controlled synthesis of 3D hierarchical MnO_2 nanostructures for electrochemical supercapacitors. Cryst Growth Des, 2009, 9: 528–533
75 Yu P, Zhang X, Chen Y, *et al.* Preparation and pseudo-capacitance of birnessite-type MnO_2 nanostructures *via* microwave-assisted emulsion method. Mater Chem Phys, 2009, 118: 303–307
76 Yuan C, Hou L, Yang L, *et al.* Facile interfacial synthesis of flower-like hierarchical a-MnO_2 sub-microspherical superstructures constructed by two-dimension mesoporous nanosheets and their application in electrochemical capacitors. J Mater Chem, 2011, 21: 16035–16041
77 Sumboja A, Tefashe UM, Wittstock G, *et al.* Monitoring electroactive ions at manganese dioxide pseudocapacitive electrodes with scanning electrochemical microscope for supercapacitor electrodes. J Power Sources, 2012, 207: 205–211
78 Yu LL, Zhu JJ, Zhao JT. Beta-manganese dioxide nanoflowers self-assembled by ultrathin nanoplates with enhanced supercapacitive performance. J Mater Chem A, 2014, 2: 9353–9360
79 Jiang H, Sun T, Li C, *et al.* Hierarchical porous nanostructures assembled from ultrathin MnO_2 nanoflakes with enhanced supercapacitive performances. J Mater Chem, 2012, 22: 2751–2756
80 Bag S, Raj CR. Facile shape-controlled growth of hierarchical mesoporous δ-MnO_2 for the development of asymmetric supercapacitors. J Mater Chem A, 2016, 4: 8384–8394
81 Liu B, Zhang X, Shioyama H, *et al.* Converting cobalt oxide subunits in cobalt metal-organic framework into agglomerated Co_3O_4 nanoparticles as an electrode material for lithium ion battery. J Power Sources, 2010, 195: 857–861
82 Yuan C, Yang L, Hou L, *et al.* Growth of ultrathin mesoporous Co_3O_4 nanosheet arrays on Ni foam for high-performance electrochemical capacitors. Energ Environ Sci, 2012, 5: 7883–7887
83 Zheng M, Cao J, Liao S, *et al.* Preparation of mesoporous Co_3O_4 nanoparticles *via* solid−liquid route and effects of calcination temperature and textural parameters on their electrochemical capacitive behaviors. J Phys Chem C, 2009, 113: 3887–3894
84 Yang Q, Lu Z, Chang Z, *et al.* Hierarchical Co_3O_4 nanosheet@nanowire arrays with enhanced pseudocapacitive performance. RSC Adv, 2012, 2: 1663–1668

85 Yuan C, Yang L, Hou L, *et al.* Large-scale Co_3O_4 nanoparticles growing on nickel sheets *via* a one-step strategy and their ultrahighly reversible redox reaction toward supercapacitors. J Mater Chem, 2011, 21: 18183–18185

86 Xia X, Tu J, Mai Y, *et al.* Self-supported hydrothermal synthesized hollow Co_3O_4 nanowire arrays with high supercapacitor capacitance. J Mater Chem, 2011, 21: 9319–9325

87 Zheng Y, Li Z, Xu J, *et al.* Multi-channeled hierarchical porous carbon incorporated Co_3O_4 nanopillar arrays as 3D binder-free electrode for high performance supercapacitors. Nano Energ, 2016, 20: 94–107

88 Yadav AA, Chavan UJ. Electrochemical supercapacitive performance of spray deposited Co_3O_4 thin film nanostructures. Electrochim Acta, 2017, 232: 370–376

89 Xiong S, Yuan C, Zhang X, *et al.* Controllable synthesis of mesoporous Co_3O_4 nanostructures with tunable morphology for application in supercapacitors. Chem Eur J, 2009, 15: 5320–5326

90 Zhu T, Chen JS, Lou XW. Shape-controlled synthesis of porous Co_3O_4 nanostructures for application in supercapacitors. J Mater Chem, 2010, 20: 7015–7020

91 Duan BR, Cao Q. Hierarchically porous Co_3O_4 film prepared by hydrothermal synthesis method based on colloidal crystal template for supercapacitor application. Electrochim Acta, 2012, 64: 154–161

92 Luo F, Li J, Lei Y, *et al.* Three-dimensional enoki mushroom-like Co_3O_4 hierarchitectures constructed by one-dimension nanowires for high-performance supercapacitors. Electrochim Acta, 2014, 135: 495–502

93 Zhou X, Shen X, Xia Z, *et al.* Hollow fluffy Co_3O_4 cages as efficient electroactive materials for supercapacitors and oxygen evolution reaction. ACS Appl Mater Interfaces, 2015, 7: 20322–20331

94 Qian Y, Liu R, Wang Q, *et al.* Efficient synthesis of hierarchical NiO nanosheets for high-performance flexible all-solid-state supercapacitors. J Mater Chem A, 2014, 2: 10917–10922

95 Meher SK, Justin P, Ranga Rao G. Microwave-mediated synthesis for improved morphology and pseudocapacitance performance of nickel oxide. ACS Appl Mater Interfaces, 2011, 3: 2063–2073

96 Huang ML, Gu CD, Ge X, *et al.* NiO nanoflakes grown on porous graphene frameworks as advanced electrochemical pseudocapacitor materials. J Power Sources, 2014, 259: 98–105

97 Li J, Zhao W, Huang F, *et al.* Single-crystalline $Ni(OH)_2$ and NiO nanoplatelet arrays as supercapacitor electrodes. Nanoscale, 2011, 3: 5103–5109

98 Liu T, Jiang C, Cheng B, *et al.* Hierarchical flower-like C/NiO composite hollow microspheres and its excellent supercapacitor performance. J Power Sources, 2017, 359: 371–378

99 Lu Z, Chang Z, Liu J, *et al.* Stable ultrahigh specific capacitance of NiO nanorod arrays. Nano Res, 2011, 4: 658–665

100 An L, Xu K, Li W, *et al.* Exceptional pseudocapacitive properties of hierarchical NiO ultrafine nanowires grown on mesoporous NiO nanosheets. J Mater Chem A, 2014, 2: 12799–12804

101 Cao F, Pan GX, Xia XH, *et al.* Synthesis of hierarchical porous NiO nanotube arrays for supercapacitor application. J Power Sources, 2014, 264: 161–167

102 Yang Z, Xu F, Zhang W, *et al.* Controllable preparation of multishelled NiO hollow nanospheres *via* layer-by-layer self-assembly for supercapacitor application. J Power Sources, 2014, 246: 24–31

103 Meng G, Yang Q, Wu X, *et al.* Hierarchical mesoporous NiO nanoarrays with ultrahigh capacitance for aqueous hybrid supercapacitor. Nano Energ, 2016, 30: 831–839

104 Yang Y, Pei L, Xu X, *et al.* *In-situ* growth of self-assembled 3D Cu_2O@Cu foam with enhanced electrochemical properties. Electrochim Acta, 2016, 221: 56–61

105 Dong C, Wang Y, Xu J, *et al.* 3D binder-free Cu_2 O@Cu nanoneedle arrays for high-performance asymmetric supercapacitors. J Mater Chem A, 2014, 2: 18229–18235

106 Deng MJ, Wang CC, Ho PJ, *et al.* Facile electrochemical synthesis of 3D nano-architectured CuO electrodes for high-performance supercapacitors. J Mater Chem A, 2014, 2: 12857–12865

107 He D, Xing S, Sun B, *et al.* Design and construction of three-dimensional flower-like CuO hierarchical nanostructures on copper foam for high performance supercapacitor. Electrochim Acta, 2016, 210: 639–645

108 Lu Y, Yan H, Qiu K, *et al.* Hierarchical porous CuO nanostructures with tunable properties for high performance supercapacitors. RSC Adv, 2015, 5: 10773–10781

109 Li L, Zhang X, Zhang Z, *et al.* A bismuth oxide nanosheet-coated electrospun carbon nanofiber film: a free-standing negative electrode for flexible asymmetric supercapacitors. J Mater Chem A, 2016, 4: 16635–16644

110 Fan HT, Teng XM, Pan SS, *et al.* Optical properties of δ-Bi_2O_3 thin films grown by reactive sputtering. Appl Phys Lett, 2005, 87: 231916

111 He W, Qin W, Wu X, *et al.* The photocatalytic properties of bismuth oxide films prepared through the sol-gel method. Thin Solid Films, 2007, 515: 5362–5365

112 Gujar TP, Shinde VR, Lokhande CD, *et al.* Electrosynthesis of Bi_2O_3 thin films and their use in electrochemical supercapacitors. J Power Sources, 2006, 161: 1479–1485

113 Zheng FL, Li GR, Ou YN, *et al.* Synthesis of hierarchical rippled Bi_2O_3 nanobelts for supercapacitor applications. Chem Commun, 2010, 46: 5021–5023

114 Su H, Cao S, Xia N, *et al.* Controllable growth of Bi_2O_3 with rod-like structures *via* the surfactants and its electrochemical properties. J Appl Electrochem, 2014, 44: 735–740

115 Zhou J, Huang Y, Cao X, *et al.* Two-dimensional $NiCo_2O_4$ nanosheet-coated three-dimensional graphene networks for high-rate, long-cycle-life supercapacitors. Nanoscale, 2015, 7: 7035–7039

116 Ma FX, Yu L, Xu CY, *et al.* Self-supported formation of hierarchical $NiCo_2O_4$ tetragonal microtubes with enhanced electrochemical properties. Energ Environ Sci, 2016, 9: 862–866

117 Gao G, Wu HB, Ding S, *et al.* Hierarchical $NiCo_2O_4$ nanosheets grown on Ni nanofoam as high-performance electrodes for supercapacitors. Small, 2015, 11: 804–808

118 Yuan C, Li J, Hou L, *et al.* Ultrathin mesoporous $NiCo_2O_4$ nanosheets supported on ni foam as advanced electrodes for supercapacitors. Adv Funct Mater, 2012, 22: 4592–4597

119 Wei TY, Chen CH, Chien HC, *et al.* A cost-effective supercapacitor material of ultrahigh specific capacitances: spinel nickel cobaltite aerogels from an epoxide-driven sol-gel process. Adv Mater, 2010, 22: 347–351

120 Zou R, Xu K, Wang T, *et al.* Chain-like $NiCo_2O_4$ nanowires with different exposed reactive planes for high-performance supercapacitors. J Mater Chem A, 2013, 1: 8560–8566

121 Jiang H, Ma J, Li C. Hierarchical porous $NiCo_2O_4$ nanowires for high-rate supercapacitors. Chem Commun, 2012, 48: 4465–4467

122 Wang Q, Liu B, Wang X, *et al.* Morphology evolution of urchin-like $NiCo_2O_4$ nanostructures and their applications as psuedo-

capacitors and photoelectrochemical cells. J Mater Chem, 2012, 22: 21647–21653
123 Guo J, Yin Z, Zang X, *et al.* Facile one-pot synthesis of $NiCo_2O_4$ hollow spheres with controllable number of shells for high-performance supercapacitors. Nano Res, 2017, 10: 405–414
124 Lei Y, Li J, Wang Y, *et al.* Rapid microwave-assisted green synthesis of 3D hierarchical flower-shaped $NiCo_2O_4$ microsphere for high-performance supercapacitor. ACS Appl Mater Interfaces, 2014, 6: 1773–1780
125 Zhou Q, Xing J, Gao Y, *et al.* Ordered assembly of $NiCo_2O_4$ multiple hierarchical structures for high-performance pseudocapacitors. ACS Appl Mater Interfaces, 2014, 6: 11394–11402
126 Xu X, Zhou H, Ding S, *et al.* The facile synthesis of hierarchical NiCoO2 nanotubes comprised ultrathin nanosheets for supercapacitors. J Power Sources, 2014, 267: 641–647
127 Butt FK, Tahir M, Cao C, *et al.* Synthesis of novel ZnV_2O_4 hierarchical nanospheres and their applications as electrochemical supercapacitor and hydrogen storage material. ACS Appl Mater Interfaces, 2014, 6: 13635–13641
128 Liu J, Zheng M, Shi X, *et al.* Amorphous FeOOH quantum dots assembled mesoporous film anchored on graphene nanosheets with superior electrochemical performance for supercapacitors. Adv Funct Mater, 2016, 26: 919–930
129 Liu L, Guo H, Liu J, *et al.* Self-assembled hierarchical yolk–shell structured NiO@C from metal–organic frameworks with outstanding performance for lithium storage. Chem Commun, 2014, 50: 9485–9488
130 Yu L, Zhang G, Yuan C, *et al.* Hierarchical $NiCo_2O_4$@MnO_2 core–shell heterostructured nanowire arrays on Ni foam as high-performance supercapacitor electrodes. Chem Commun, 2013, 49: 137–139
131 Shin DH, Lee JS, Jun J, *et al.* Fabrication of amorphous carbon-coated NiO nanofibers for electrochemical capacitor applications. J Mater Chem A, 2014, 2: 3364–3371
132 Xia H, Hong C, Li B, *et al.* Facile synthesis of hematite quantum-dot/functionalized graphene-sheet composites as advanced anode materials for asymmetric supercapacitors. Adv Funct Mater, 2015, 25: 627–635
133 Wang K, Yang J, Zhu J, *et al.* General solution-processed formation of porous transition-metal oxides on exfoliated molybdenum disulfides for high-performance asymmetric supercapacitors. J Mater Chem A, 2017, 5: 11236–11245
134 Zhang Y, Zheng M, Qu M, *et al.* Core–shell $Co_{11}(HPO_3)_8(OH)_6$–Co_3O_4 hybrids for high-performance flexible all-solid-state asymmetric supercapacitors. J Alloys Compd, 2015, 651: 214–221
135 Zhou M, Lu F, Shen X, *et al.* One-pot construction of three dimensional $CoMoO_4$/Co_3O_4 hybrid nanostructures and their application in supercapacitors. J Mater Chem A, 2015, 3: 21201–21210
136 Li C, Balamurugan J, Thanh TD, *et al.* 3D hierarchical CoO@MnO_2 core–shell nanohybrid for high-energy solid state asymmetric supercapacitors. J Mater Chem A, 2017, 5: 397–408
137 Zhu J, Tang S, Xie H, *et al.* Hierarchically porous MnO_2 microspheres doped with homogeneously distributed Fe_3O_4 nanoparticles for supercapacitors. ACS Appl Mater Interfaces, 2014, 6: 17637–17646
138 Kong D, Luo J, Wang Y, *et al.* Three-dimensional Co_3O_4@MnO_2 hierarchical nanoneedle arrays: morphology control and electrochemical energy storage. Adv Funct Mater, 2014, 24: 3815–3826
139 Ge H, Wang C, Yin L. Hierarchical $Cu_{0.27}Co_{2.73}O_4$/MnO_2 nanorod arrays grown on 3D nickel foam as promising electrode materials for electrochemical capacitors. J Mater Chem A, 2015, 3: 17359–17368
140 Bao F, Zhang Z, Guo W, *et al.* Facile synthesis of three dimensional $NiCo_2O_4$@MnO_2 core–shell nanosheet arrays and its supercapacitive performance. Electrochim Acta, 2015, 157: 31–40
141 Zhang Y, Wang B, Liu F, *et al.* Full synergistic contribution of electrodeposited three-dimensional $NiCo_2O_4$@MnO_2 nanosheet networks electrode for asymmetric supercapacitors. Nano Energ, 2016, 27: 627–637
142 Zhu J, Xu Z, Lu B. Ultrafine Au nanoparticles decorated $NiCo_2O_4$ nanotubes as anode material for high-performance supercapacitor and lithium-ion battery applications. Nano Energ, 2014, 7: 114–123
143 Han N, Cao S, Han J, *et al.* Surface cavities of $Ni(OH)_2$ nanowires can host Au nanoparticles as supported catalysts with high catalytic activity and stability. J Mater Chem A, 2016, 4: 2590–2596
144 Hu H, Pei Z, Fan H, *et al.* 3D interdigital Au/MnO_2/Au stacked hybrid electrodes for on-chip microsupercapacitors. Small, 2016, 12: 3059–3069
145 Qu B, Hu L, Chen Y, *et al.* Rational design of Au–NiO hierarchical structures with enhanced rate performance for supercapacitors. J Mater Chem A, 2013, 1: 7023–7026
146 Liu S, Guo S, Sun S, *et al.* Dumbbell-like Au-Fe_3O_4 nanoparticles: a new nanostructure for supercapacitors. Nanoscale, 2015, 7: 4890–4893
147 Li W, Li G, Sun J, *et al.* Hierarchical heterostructures of MnO_2 nanosheets or nanorods grown on Au-coated Co_3O_4 porous nanowalls for high-performance pseudocapacitance. Nanoscale, 2013, 5: 2901–2908
148 Li Q, Wang ZL, Li GR, *et al.* Design and synthesis of MnO_2/Mn/MnO_2 sandwich-structured nanotube arrays with high supercapacitive performance for electrochemical energy storage. Nano Lett, 2012, 12: 3803–3807
149 Bao L, Zang J, Li X. Flexible Zn_2SnO_4/MnO_2 core/shell nanocable −carbon microfiber hybrid composites for high-performance supercapacitor electrodes. Nano Lett, 2011, 11: 1215–1220
150 Xia X, Tu J, Zhang Y, *et al.* High-quality metal oxide core/shell nanowire arrays on conductive substrates for electrochemical energy storage. ACS Nano, 2012, 6: 5531–5538
151 Zheng X, Yan X, Sun Y, *et al.* Au-embedded ZnO/NiO hybrid with excellent electrochemical performance as advanced electrode materials for supercapacitor. ACS Appl Mater Interfaces, 2015, 7: 2480–2485
152 Xia X, Tu J, Zhang Y, *et al.* Porous hydroxide nanosheets on preformed nanowires by electrodeposition: branched nanoarrays for electrochemical energy storage. Chem Mater, 2012, 24: 3793–3799
153 Fan W, Xia YY, Tjiu WW, *et al.* Nitrogen-doped graphene hollow nanospheres as novel electrode materials for supercapacitor applications. J Power Sources, 2013, 243: 973–981
154 Peng L, Peng X, Liu B, *et al.* Ultrathin two-dimensional MnO_2/graphene hybrid nanostructures for high-performance, flexible planar supercapacitors. Nano Lett, 2013, 13: 2151–2157
155 Qu L, Zhao Y, Khan AM, *et al.* Interwoven three-dimensional architecture of cobalt oxide nanobrush-graphene@$Ni_xCo_{2x}(OH)_{6x}$ for high-performance supercapacitors. Nano Lett, 2015, 15: 2037–2044
156 Xia W, Mahmood A, Zou R, *et al.* Metal–organic frameworks and

their derived nanostructures for electrochemical energy storage and conversion. Energ Environ Sci, 2015, 8: 1837–1866
157 Zhu G, He Z, Chen J, *et al.* Highly conductive three-dimensional MnO_2–carbon nanotube–graphene–Ni hybrid foam as a binder-free supercapacitor electrode. Nanoscale, 2014, 6: 1079–1085
158 Xie J, Sun X, Zhang N, *et al.* Layer-by-layer β-$Ni(OH)_2$/graphene nanohybrids for ultraflexible all-solid-state thin-film supercapacitors with high electrochemical performance. Nano Energ, 2013, 2: 65–74
159 Zhang W, Quan B, Lee C, *et al.* One-step facile solvothermal synthesis of copper ferrite–graphene composite as a high-performance supercapacitor material. ACS Appl Mater Interfaces, 2015, 7: 2404–2414
160 Kumar R, Dubey PK, Singh RK, *et al.* Catalyst-free synthesis of a three-dimensional nanoworm-like gallium oxide–graphene nanosheet hybrid structure with enhanced optical properties. RSC Adv, 2016, 6: 17669–17677
161 Kumar R, Savu R, Joanni E, *et al.* Fabrication of interdigitated micro-supercapacitor devices by direct laser writing onto ultrathin, flexible and free-standing graphite oxide films. RSC Adv, 2016, 6: 84769–84776
162 Kumar R, Singh RK, Dubey PK, *et al.* Freestanding 3D graphene-nickel encapsulated nitrogen-rich aligned bamboo like carbon nanotubes for high-performance supercapacitors with robust cycle stability. Adv Mater Interfaces, 2015, 2: 1500191
163 Singh RK, Kumar R, Singh DP. Graphene oxide: strategies for synthesis, reduction and frontier applications. RSC Adv, 2016, 6: 64993–65011
164 Kumar R, Kim HJ, Park S, *et al.* Graphene-wrapped and cobalt oxide-intercalated hybrid for extremely durable super-capacitor with ultrahigh energy and power densities. Carbon, 2014, 79: 192–202
165 Kumar R, Singh RK, Savu R, *et al.* Microwave-assisted synthesis of void-induced graphene-wrapped nickel oxide hybrids for supercapacitor applications. RSC Adv, 2016, 6: 26612–26620
166 Kumar R, Singh RK, Vaz AR, *et al.* Self-assembled and one-step synthesis of interconnected 3D network of Fe_3O_4/reduced graphene oxide nanosheets hybrid for high-performance supercapacitor electrode. ACS Appl Mater Interfaces, 2017, 9: 8880–8890
167 Fan L, Tang L, Gong H, *et al.* Carbon-nanoparticles encapsulated in hollow nickel oxides for supercapacitor application. J Mater Chem, 2012, 22: 16376–16381
168 Huang SZ, Cai Y, Jin J, *et al.* Hierarchical mesoporous urchin-like Mn_3O_4/carbon microspheres with highly enhanced lithium battery performance by *in-situ* carbonization of new lamellar manganese alkoxide (Mn-DEG). Nano Energ, 2015, 12: 833–844
169 Zheng M, Qiu D, Zhao B, *et al.* Mesoporous iron oxide directly anchored on a graphene matrix for lithium-ion battery anodes with enhanced strain accommodation. RSC Adv, 2013, 3: 699–703
170 Zhang Z, Xiao F, Wang S. Hierarchically structured MnO_2/graphene/carbon fiber and porous graphene hydrogel wrapped copper wire for fiber-based flexible all-solid-state asymmetric supercapacitors. J Mater Chem A, 2015, 3: 11215–11223
171 Ge J, Yao HB, Hu W, *et al.* Facile dip coating processed graphene/MnO_2 nanostructured sponges as high performance supercapacitor electrodes. Nano Energ, 2013, 2: 505–513
172 Kumar R, Singh RK, Dubey PK, *et al.* Self-assembled hierarchical formation of conjugated 3D cobalt oxide nanobead–CNT–graphene nanostructure using microwaves for high-performance supercapacitor electrode. ACS Appl Mater Interfaces, 2015, 7: 15042–15051
173 Zhang J, Zhao X, Huang Z, *et al.* High-performance all-solid-state flexible supercapacitors based on manganese dioxide/carbon fibers. Carbon, 2016, 107: 844–851
174 Javed MS, Zhang C, Chen L, *et al.* Hierarchical mesoporous $NiFe_2O_4$ nanocone forest directly growing on carbon textile for high performance flexible supercapacitors. J Mater Chem A, 2016, 4: 8851–8859
175 Yue S, Tong H, Lu L, *et al.* Hierarchical $NiCo_2O_4$ nanosheets/nitrogen doped graphene/carbon nanotube film with ultrahigh capacitance and long cycle stability as a flexible binder-free electrode for supercapacitors. J Mater Chem A, 2017, 5: 689–698
176 Hou S, Zhang G, Zeng W, *et al.* Hierarchical core–shell structure of ZnO nanorod@NiO/MoO_2 composite nanosheet arrays for high-performance supercapacitors. ACS Appl Mater Interfaces, 2014, 6: 13564–13570
177 Mai LQ, Yang F, Zhao YL, *et al.* Hierarchical $MnMoO_4$/$CoMoO_4$ heterostructured nanowires with enhanced supercapacitor performance. Nat Commun, 2011, 2: 381
178 Ding Y, Wan Y, Min YL, *et al.* General synthesis and phase control of metal molybdate hydrates $MMoO_4 \cdot nH_2O$ (M = Co, Ni, Mn, n = 0, 3/4, 1) nano/microcrystals by a hydrothermal approach: magnetic, photocatalytic, and electrochemical properties. Inorg Chem, 2008, 47: 7813–7823
179 Wang J, Zhang X, Wei Q, *et al.* 3D self-supported nanopine forest-like Co_3O_4@$CoMoO_4$ core–shell architectures for high-energy solid state supercapacitors. Nano Energ, 2016, 19: 222–233
180 Lu Z, Yang Q, Zhu W, *et al.* Hierarchical Co_3O_4@Ni-Co-O supercapacitor electrodes with ultrahigh specific capacitance per area. Nano Res, 2012, 5: 369–378
181 Yang Q, Lu Z, Li T, *et al.* Hierarchical construction of core–shell metal oxide nanoarrays with ultrahigh areal capacitance. Nano Energ, 2014, 7: 170–178
182 Wu X, Lu Z, Zhu W, *et al.* High-performance aqueous battery with double hierarchical nanoarrays. Nano Energ, 2014, 10: 229–234
183 Lin YG, Hsu YK, Lin YC, *et al.* Hierarchical Fe_2O_3 nanotube/nickel foam electrodes for electrochemical energy storage. Electrochim Acta, 2016, 216: 287–294
184 Wu Q, Chen M, Chen K, *et al.* Fe_3O_4-based core/shell nanocomposites for high-performance electrochemical supercapacitors. J Mater Sci, 2016, 51: 1572–1580
185 Liu Z, Tian X, Xu X, *et al.* Capacitance and voltage matching between MnO_2 nanoflake cathode and Fe_2O_3 nanoparticle anode for high-performance asymmetric micro-supercapacitors. Nano Res, 2017, 10: 2471–2481
186 Lu Z, Wu X, Lei X, *et al.* Hierarchical nanoarray materials for advanced nickel–zinc batteries. Inorg Chem Front, 2015, 2: 184–187

Acknowledgements This work was supported by the National Natural Science Foundation of China (51202106, 21671170 and 21673203) and New Century Excellent Talents of the University in China (NCET-13-0645), the Innovation Scientists and Technicians Troop Construction Projects of Henan Province (164200510018), the Plan for Scientific Innovation Talent of Henan Province, the Program for Innovative Research Team (in Science and Technology) in the University of Henan Province (14IRTSTHN004 and 16IRTSTHN003), the Science & Tech-

nology Foundation of Henan Province (122102210253 and 13A150019), the Science & Technology Foundation of Jiangsu Province (BK20150438), the Six Talent Plan (2015-XCL-030), and China Postdoctoral Science Foundation (2012M521115). We also acknowledge the Priority Academic Program Development of Jiangsu Higher Education Institutions and the technical support we received at the Testing Center of Yangzhou University.

Author contributions Zheng M, Xiao X and Li L organized the literatures and wrote the manuscript. Gu P participated in writing and revising the manuscript. Dai X, Tang H, Hu Q, and Xue H revised the manuscript. Pang H provided the overall concept and revised the manuscript. All authors participated in the general discussion.

Conflict of interest The authors declare that they have no conflict of interest.

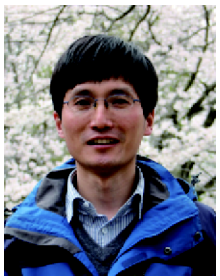

Mingbo Zheng received his PhD in material processing engineering from Nanjing University of Aeronautics and Astronautics in 2009. He was a postdoctoral researcher at Nanjing University from 2009 to 2012. He was an associate researcher at Nanjing University from 2012 to 2015. He is currently an associate professor at Yanzhou University. His research interests are in the field of materials for electrochemical energy storge, including supercapacitor, lithium-ion battery, and lithium-sulfur battery.

Huan Pang received his PhD degree from Nanjing University in 2011. He then founded his research group in Anyang Normal University where he was appointed as a distinguished professor in 2013. He has now jointed Yangzhou University as a University Distinguished Professor. His research interests include the development of inorganic nanostructures and their applications in flexible electronics with a focus on energy devices.

多级纳米结构过渡金属氧化物作为超级电容器电极材料的应用

郑明波, 肖潇, 李露露, 顾鹏, 戴晓, 唐浩, 胡钦, 薛怀国, 庞欢*

摘要 为了应对化石燃料短缺与日益严重的环境污染问题, 开发高效、清洁、可持续的电化学储能技术已迫在眉睫. 超级电容器, 由于其功率密度高、充放电时间短、循环寿命长等特点, 已得到广泛关注. 多种过渡金属氧化物已被作为超级电容器电极材料进行了深入研究. 为了进一步提高性能, 具有多级纳米结构的过渡金属氧化物材料已成为目前超级电容器领域的研究热点. 多级纳米结构不仅可以为电化学反应提供更多活性位点, 同时还可以缩短离子的传输路径. 本综述对多级纳米结构过渡金属氧化物在超级电容器电极材料方面的应用, 进行了系统的总结与评价, 主要包括: 合成方法、成分、结构和电化学性能. 此外, 对该领域的进一步发展进行了展望.

